Fragmentation of a foreland basin in response to out-of-sequence basement uplifts and structural reactivation: El Cajón–Campo del Arenal basin, NW Argentina

Estelle Mortimer[†]
Barbara Carrapa
Institut für Geowissenschaften, Universität Potsdam, Karl-Liebknecht-Strasse 24/25, Potsdam 14476, Germany

Isabelle Coutand
Université des Sciences et Technologies de Lille 1, UMR-CNRS 8110, Villeneuve d'Ascq cedex, France

Lindsay Schoenbohm[‡]
Edward R. Sobel
Institut für Geowissenschaften, Universität Potsdam, Karl-Liebknecht-Strasse 24/25, Potsdam 14476, Germany

José Sosa Gomez
Universidad Nacional de Tucumán, Facultad de Ciencias Naturales, Miguel Lillo 205, 4000 Tucumán, Argentina

Manfred R. Strecker
Institut für Geowissenschaften, Universität Potsdam, Karl-Liebknecht-Strasse 24/25, Potsdam 14476, Germany

ABSTRACT

The style and mechanisms by which a foreland region is incorporated into an orogen depends on the tectonic style, effectiveness of uplift, and dynamic subsidence. Classical foreland-basin models reflect a self-similar propagation of deformation into the foreland in a thin-skinned thrust-belt setting governed by wedge mechanics. Thick-skinned foreland regions, which are characterized by high-angle reverse-fault–bounded basement uplifts and intervening basins, however, do not fit this idealized model. Unlike thin-skinned tectonic provinces, deformation and uplift in these regions may be highly variable in time and space. Furthermore, deformation patterns may be complicated by the presence of preexisting structures, particularly those which lie at orientations that enable them to be reactivated and utilized to accommodated deformation under compression.

The Neogene El Cajón–Campo del Arenal basin is one of a series of basins located along the eastern margin of the Puna Plateau within the Sierras Pampeanas, a region that is composed of a thick-skinned foreland fragmented by reverse-fault–bounded basement uplifts that regionally characterize an eastward-younging trend. This region is superimposed onto the Cretaceous Salta Rift province, which provides a series of preexisting structures that may potentially be reactivated. The basin is located along the eastern margin of the Puna Plateau, an integral component of the Andean orogen, which includes several filled, uplifted, and internally drained Cenozoic intraplateau basins. Structural and sedimentological similarities exist between basins along the margin of the Puna and those within it. Understanding the evolution of foreland basins, such as the El Cajón–Campo del Arenal basin, provides possible mechanisms for the development and incorporation of marginal basins into orogenic belts, and in the case of the Andean orogen, the potential for these basins to be incorporated into the plateau.

Our analysis, which integrates seismic, sedimentary, and thermochronological data, characterizes the evolution of this basin and surrounding ranges. The appearance in the sedimentary section of a distinct grain-age population derived from the basement erosion surface constrains the uplift and erosion of an out-of-sequence intrabasin high to ca. 6 Ma. The basin fill, therefore, records an evolution from an undeformed foreland to one that is compartmentalized by basement uplifts and that is incorporated into the greater orogenic structure. The data reveal the importance of the reactivation of preexisting structures along the basin margin in creating east-dipping structures in a generally west-dipping domain. These opposing faults on the basin margin consequently caused the out-of-sequence uplift of the intrabasin range, the Sierra de Quilmes. The Sierra de Quilmes fragments the foreland and, because its position is locked by loads to the west and east, creates increased deformation within the basin, basin fill, uplift, and incorporation into the orogen. Unlike basins within the plateau, however, the El Cajón–Campo del Arenal basin has been re-excavated and integrated once more into the foreland drainage network.

Keywords: foreland basin, basement uplift, stratigraphy, reactivation, thermochronology.

INTRODUCTION

The formation of foreland basins and their subsequent incorporation into deformation zones governed by critical Coulomb wedge

[†]E-mail: estellem@geo.uni-potsdam.de.
[‡]Present address: Department of Geological Sciences, Ohio State University, 275 Mendenhall Laboratory, 125 S. Oval Mall, Columbus, Ohio 43210, USA.

GSA Bulletin; May/June 2007; v. 119; no. 5/6; p. 637–653; doi: 10.1130/B25884.1; 9 figures; 3 tables.

mechanics are integral facets of the evolution of many orogens and results in wedge-shaped, internally deformed thrust belts underlain by décollements (Davis et al., 1983; Dahlen et al., 1984). Foreland basins are the flexurally driven elongate depressions that form between a linear orogenic belt and a stable craton (Jordan, 1981, 1995; DeCelles and Giles, 1996). In an ideal setting, according to the model of Flemings and Jordan (1989), the thrust load is consistent along strike, and the thrust front moves toward the foreland, while foreland basin subsidence and fill would mimic the behavior of the advancing thrust front. It has, however, been demonstrated that this view of a wedge-shaped foreland basin is simplified (e.g., DeCelles and Giles, 1996; Jordan et al., 2001) and that differences in stratal thickness and basin geometry can result from a number of external factors. The process by which a foreland foredeep basin (sensu DeCelles and Giles, 1996) becomes entrained into an orogenic wedge depends on the relative effectiveness of basin uplift due to propagation of the orogenic wedge versus dynamic basin subsidence due to the flexural load combined with far field stresses (DeCelles and Giles, 1996). These models of foreland basin development are based upon a thin-skinned tectonic setting, in which a sedimentary fold-and-thrust belt comprises an orogenic wedge. In such an environment, it is possible that basement rocks may become involved and uplifted within the fold-and-thrust belt where there are interior ramp-supported uplifts (Schmitt and Steidtmann, 1990). This process is, however, a passive process involving the uplift of existing thrust plates in a younger thrust.

In stark contrast, thick-skinned foreland deformation involves basement rocks being actively uplifted and incorporated into the orogen on high-angle reverse faults. In this setting, the propagation and pattern of deformation may not follow the principles of wedge mechanics of thin-skinned fold-and-thrust belts (Hilley et al., 2005). In particular, in situations where crustal heterogeneities are very pronounced and/or where the geodynamic conditions are conducive to widespread basement-cored uplifts, the deformation that occurs in the foreland may be highly diachronous and spatially variable. This phenomenon of deformation being accommodated on thick-skinned basement uplifts is well exemplified in the Laramide province of the western United States (Gries, 1983; Jordan et al., 1983) and its late Cenozoic equivalent in the Sierras Pampeanas of Argentina, which spatially correlates with a subhorizontal section of oceanic Nazca plate between 27 and 33°S latitude (Dickinson and Snyder, 1978; Jordan et al., 1983; Jordan and Allmendinger, 1986; Ramos et al., 2002).

Both thin-skinned and thick-skinned foreland settings have similar characteristics: deformation propagates into the foreland; the load of the uplifted topography creates subsidence and a depozone (classically thin-skinned flexural foredeep; sensu DeCelles and Giles, 1996); the foreland is fragmented and incorporated into the orogen. In the case of thick-skinned tectonics, individual structures create localized loading and depocenters, which, if sufficient, may generate flexure. The primary difference is that in the thick-skinned scenario, such as the Sierras Pampeanas of northwest Argentina, there is no simple propagation of a classic wedge, ranges are composed of basement rocks, and range-bounding structures are typically high-angle reverse faults, often associated with reactivated preexisting structures (Marshak et al., 2000; Ramos et al., 2002; Hilley et al., 2005).

Here, we investigate a high-angle reverse-fault bounded foreland basin, the El Cajón–Campo del Arenal basin, which is located between the southeastern margin of the intra-Andean Puna Plateau and the Sierras Pampeanas of northwest Argentina (Fig 1). In contrast to regions farther north in the Andes, where a classical orogenic wedge geometry has been demonstrated (e.g., Kley et al., 1997; Horton and DeCelles, 1997; DeCelles and Horton, 2003), this region is characterized by a thick-skinned tectonic regime composed of high-angle reverse-fault–bounded basement uplifts and intervening basins. It has been likened to the Cretaceous to Eocene Laramide province of the western United States (Jordan et al., 1983; Jordan and Allmendinger, 1986), and it is similar to the basement uplifts in the Tien Shan mountains of central Asia (Burtman, 1975; Burbank et al., 1999) or the Qilian Shan at the margin of northeastern Tibet (Tapponnier et al., 1990).

Much of the region is superimposed onto the structures of the Cretaceous Salta Rift (e.g., Mon and Salfity, 1995; Davila and Astini, 2003). This thick-skinned characteristic coupled with its superposition create the opportunity for this region of the Sierras Pampeanas to undergo structural reactivation within the foreland region under compression, and the potential for deviation from the more straightforward modes of foreland evolution. The basement uplifts and intervening basins of the northwestern Sierras Pampeanas were once an integral part of an undeformed continuous foreland to the east of the basement-range uplifts that comprise the eastern border of the intra-Andean Puna Plateau.

To reconstruct the spatial and temporal evolution of the El Cajón–Campo del Arenal basin (Fig. 2) this study integrates sedimentologic, seismic-reflection, and apatite fission-track thermochronological data. From this reconstruction, this study aims (1) to characterize and propose mechanisms for the compartmentalization of the basin, and (2) to determine the pattern and timing of thrusting within the basin.

Our investigations document the transition of the basin from its initial location in the continuous foreland ahead of thick-skinned, reverse-fault–bounded basement uplifts at the southeastern margin of the Puna to its incorporation into the southern-central Andes tectonic domain as deformation propagated into the foreland. This characterization of the El Cajón–Campo del Arenal basin is used to determine: (1) how structures and sedimentary deposits evolve in a broken foreland province, and how the evolution of the basin differs from existing foreland basin models; and (2) the mechanism(s) that generates these differences, and the implications for the development of other basins along the margin of the Puna Plateau today, which will further improve our understanding of basin dynamics in response to orogen development.

GEOLOGICAL SETTING

The El Cajón–Campo Arenal basin is located east of the basement ranges that constitute the eastern margin of the Puna Plateau, in the southern-central Andes. The Puna Plateau is the second highest plateau on Earth; it is at 3.7 km mean elevation and has intervening peaks in excess of 6 km (Isacks, 1988). Along the southern margin of the plateau, in the Sierras Pampeanas and the Eastern Cordillera of Argentina, several compressional Neogene sedimentary basins record progressive uplift and deformation associated with the plateau margin (e.g., Allmendinger et al., 1997; Allmendinger, 1986; Allmendinger, et al., 1983; Bossi et al., 2000; Caminos, 1979; Jordan and Alonso, 1987; Strecker et al., 1989; Sobel et al., 2003; Hilley and Strecker, 2005). The deformation of the foreland in the Sierras Pampeanas is characterized by high-angle reverse-fault–bounded basement ranges (Jordan and Allmendinger, 1986; Ramos et al., 2002) with intervening Neogene sedimentary basins. These sedimentary units in these basins were deposited onto a polycyclic erosion surface cut into Paleozoic metamorphic basement rocks (e.g., Bossi, 1992; Jordan and Allmendinger, 1986; Jordan et al., 1989; Toselli and Rossi, 1998; Toselli et al., 1999; Sobel and Strecker, 2003). The Tertiary sedimentary rocks that overlie the Sierras Pampeanas basement are similar, although they vary in thickness and age among all of the basins (Jordan and Allmendinger, 1986; Jordan et al., 1989; Bossi, 1992). In particular, the deposition of coarsening-up alluvial sequences is recognized, and the presence of a distinctive coarse conglomerate (Punaschotter)

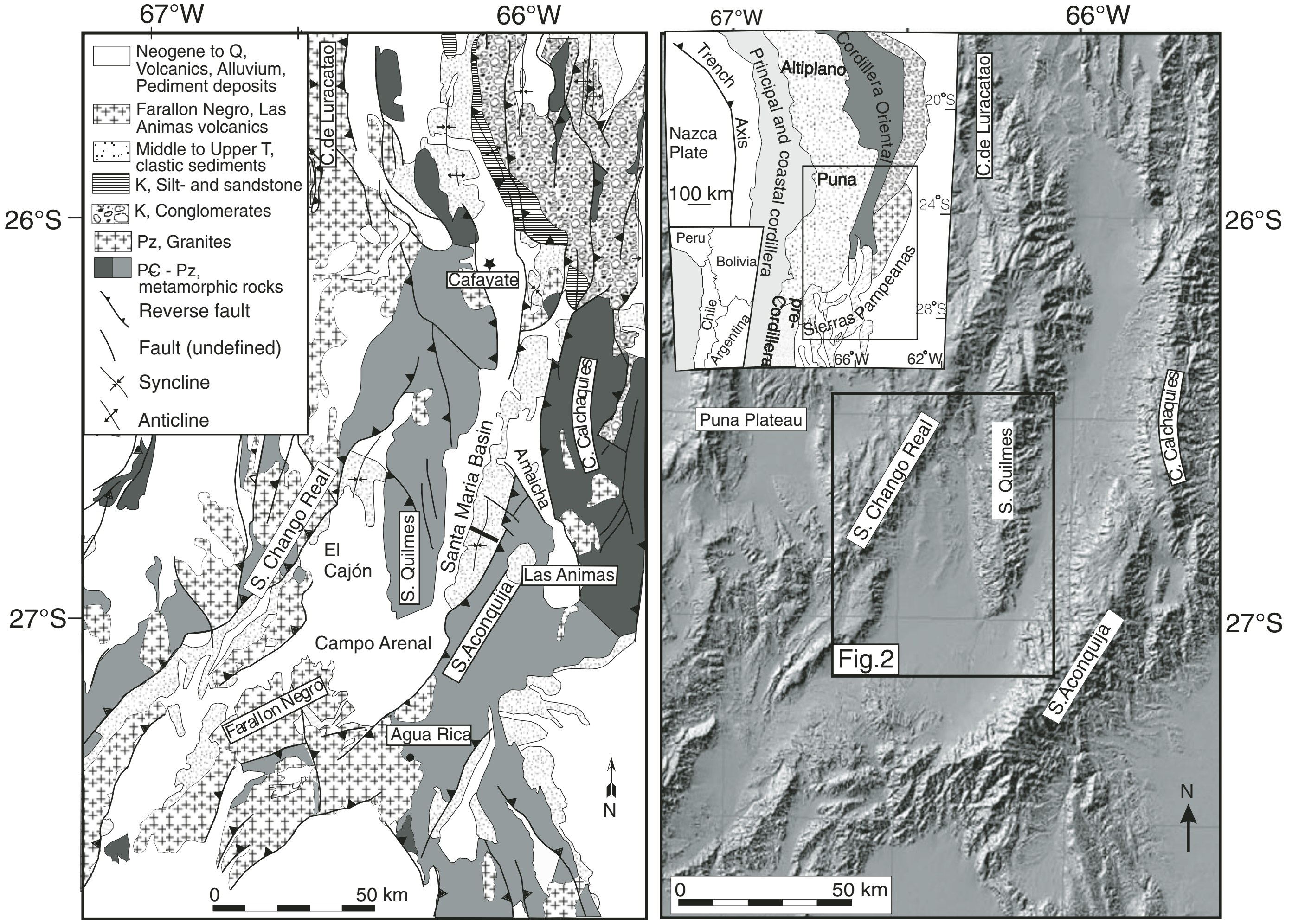

Figure 1. Geological map (left) and digital elevation model (DEM; right) of the Sierras Pampeanas, NW Argentina (see inset for exact location). The investigated Neogene compressional basin, the El Cajón–Campo Arenal basin, is located along the southeastern margin of the Puna Plateau.

that constitutes the latest Pliocene to Quaternary deposits is a common feature throughout the northwestern Sierras Pampeanas bordering the Puna Plateau (Penck, 1920; Allmendinger, 1986; Strecker et al., 1989; Bossi et al., 1997; Hilley and Strecker, 2005). The El Cajón and Campo del Arenal subbasins (Figs. 1 and 2) are the northern and southern extents of a single basin, respectively. Here, we present an analysis of the Tertiary sediments preserved in the basin fill, which record a wealth of information concerning the tectono-sedimentary history of the eastern margin of the Puna Plateau.

The El Cajón–Campo del Arenal basin (at an elevation of ~2.6 km) is bounded to the west by the Sierra de Chango Real, which has an elevation of ~4 km and forms the southeastern margin of the Puna plateau. The basin is bounded to the east by the Sierra de Quilmes, a southward-plunging basement anticline (Strecker, 1987; Strecker et al., 1989) that separates the El Cajón–Campo del Arenal basin from the Santa Maria basin to the east. The Sierra de Quilmes thus fragments this region of the former foreland and is an effective barrier to sediment transport between these basins. While there are west-dipping structures documented within Sierra de Quilmes (this study), no faults have been documented delimiting either boundary of this antiform. The Santa Maria basin is bounded to the east by Sierra de Aconquija, which has been shown to have had a significant control on sedimentation in the Santa Maria basin (Bossi et al., 1997), and was actively being exhumed from ca. 6 Ma onward (Sobel and Strecker, 2003).

METHODS

This study undertakes a multidisciplinary approach to investigate the El Cajón–Campo del Arenal basin evolution. Measured stratigraphic sections and subsurface seismic-reflection data are combined to constrain the sedimentological and structural evolution of the basin fill. These data are then integrated with apatite fission-track (AFT) data from basement ranges and detrital grains from known stratigraphic locations to evaluate the potential areas from which detrital grains were derived. This combination of techniques provides a strong methodology for determination of the timing of exhumation of surrounding ranges and their involvement in basin evolution.

Apatite fission-track (AFT) thermochronology constrains the cooling history of a range by tracking the time a sample passes through the partial annealing zone (PAZ), typically between ~110 and 60 °C (e.g., Fitzgerald et al., 1995; Gallagher et al., 1998). Apatite grains that have been exhumed to the surface, eroded, and subsequently redeposited in a sedimentary basin can be used as provenance indicators by comparing the AFT age of detrital grains with the

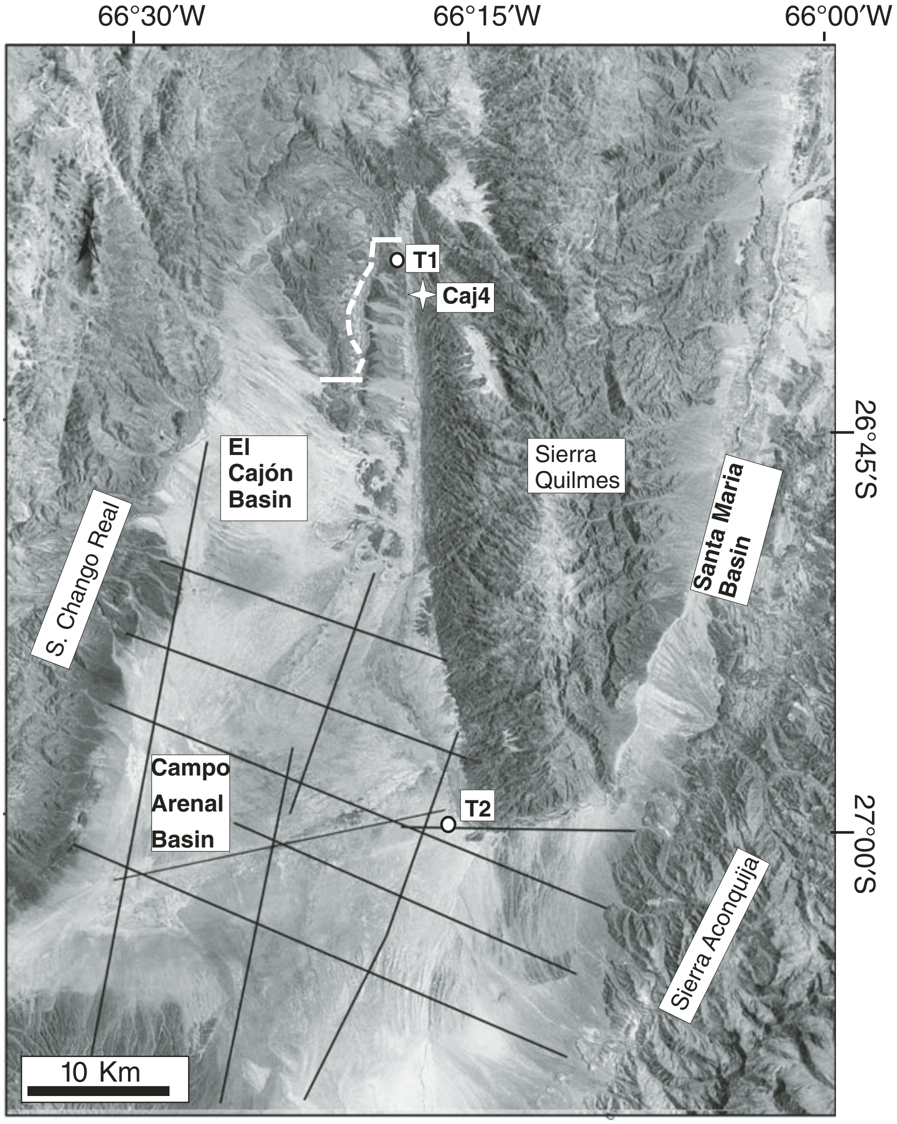

Figure 2. The El Cajón–Campo Arenal basin, Sierra Pampeanas, NW Argentina (for exact location, see also Fig. 1). This multidisciplinary study integrates seismic-reflection profiles (black lines); sedimentary sections (solid white lines correlated to basalt [dashed] flow); detrital apatite fission-track (AFT) samples collected within the sedimentary section (see Fig. 3 and Table 2 for specific location within the measured section); basement AFT sample (white star; Caj 4). The seismic data and sedimentary section are temporally constrained by two dated tuff deposits (white circles): T1 (Strecker, 1987) and T2 (Strecker et al., 1989).

AFT ages of rocks in surrounding ranges (e.g., Garver et al., 1999; Ruiz et al., 2004; Coutand et al., 2006). For fairly rapidly cooled samples, the AFT age reflects cooling through the hotter portion of the PAZ; the difference between this time and when the grain is deposited is termed the lag time (Cerveny et al., 1988). In turn, with such data, it is possible to constrain the timing and rate of exhumation of the source range. In particular, in order for a range to provide detritus, it must first be uplifted and any overlying sediment removed. Therefore, the onset of exhumation of a range can be constrained by the first appearance of grains in the basin fill with the corresponding basement source area ages.

Analysis and reduction of AFT data in this study were based on the method described in Sobel and Strecker (2003) and Coutand et al. (2006). The annealing behavior of apatite is dependent on the kinetic characteristics of the grains. In order to examine such variations, we measured etch pit diameters (Dpar; Donelick et al., 1999) for all samples. For detrital samples, grain-shape analysis was undertaken to better discriminate between different source types. Thermal modeling that combined track length, single-crystal ages, and Dpar was performed on the basement samples using the AFT Solve program (Ketcham et al., 2000). Binomial peak-fit ages (populations) for detrital samples were extracted using the Binomfit software of Brandon (2002).

BASIN STRATIGRAPHY

The sedimentary facies and architecture of the basin fill provide an important record of the spatio-temporal evolution of the basin and surrounding ranges. The El Cajón–Campo del Arenal basin has good exposure of the sedimentary fill in the northern (El Cajón) subbasin that is lacking to the south (Campo del Arenal subbasin). Therefore, while the facies of the basin fill are documented from the north of the basin, the depositional architecture is best recorded from seismic-reflection profiles in the southern subbasin.

Sedimentary Facies

Throughout much of its history, the El Cajón–Campo del Arenal basin has been dominated by a coarsening-up sequence of clastic sedimentation comprising deposits related to debris fans, alluvial fans, and floodplains. Where these sediments are exposed, in the northern (El Cajón) subbasin, two 1:50 stratigraphic sections, correlated along a continuous basalt flow, document 1200 m of Tertiary stratigraphy (Fig. 1 for location; Fig. 3) from the basal contact with basement rocks of Sierra de Quilmes to a pronounced angular unconformity. Above this unconformity lies a cobble-boulder conglomerate with a minimum thickness of 250 m. It is not the aim of this investigation to provide detailed sedimentary analyses of the basin fill, as the existing scheme of Bossi (1992) and Bossi et al. (2000) provides good interpretations and descriptions of the sediments preserved in the basin. In this study, therefore, sedimentary observations (Fig. 3) recorded in the sections are equivalent to those of Bossi (1992) and Bossi et al. (2000), and they are summarized in Table 1.

Temporal constraints on the sedimentary section are provided through dated interbedded tuff horizons. The base of the lowermost, the Peñas Azules Formation, is constrained by a tuff dated by zircon fission track at 10.7 ± 1.7 Ma (Strecker, 1987). A tuff within lacustrine sediments in the middle Playa del Zorro Formation constrains deposition to 5.7 ± 0.4 Ma (Bossi et al., 2000). The Playa del Zorro Formation is separated from the uppermost formation, the Tortoral Formation, by an

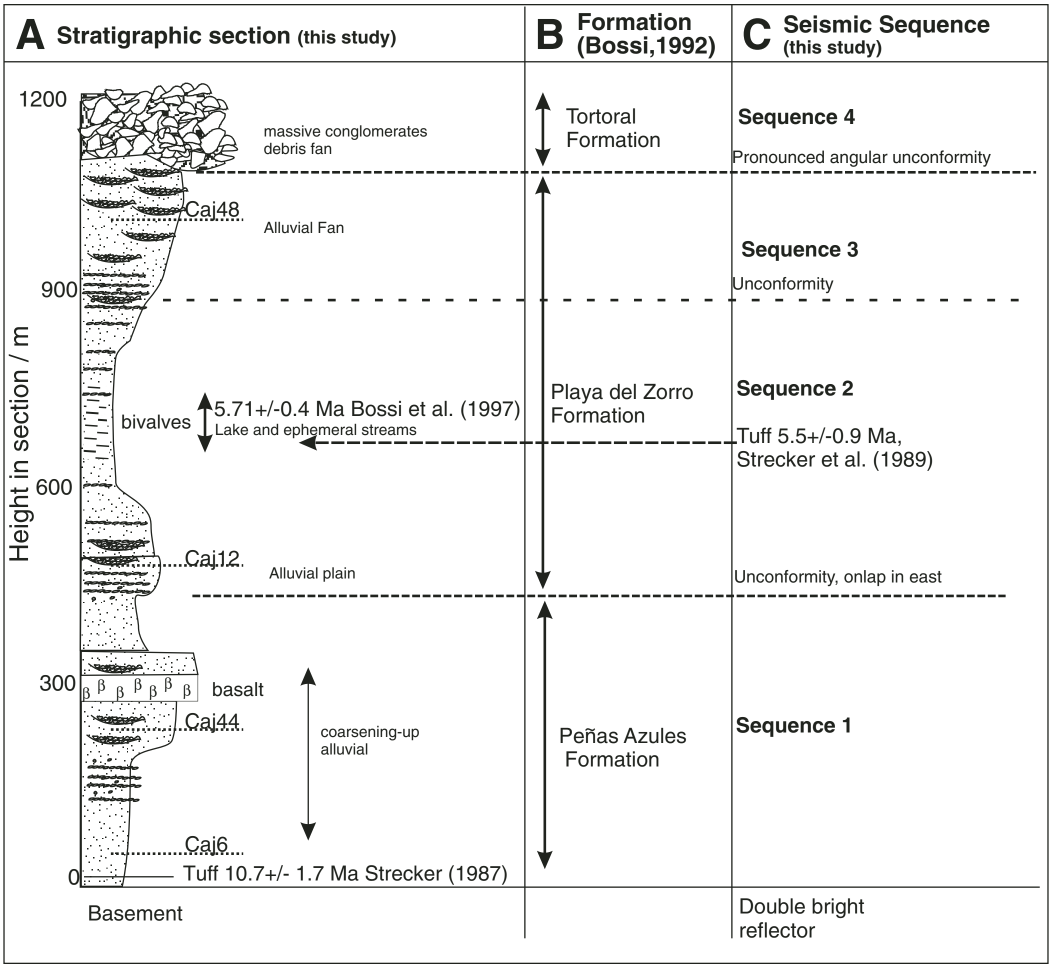

Figure 3. (A) Sedimentary logged section (see Fig. 2 for location) from the El Cajón basin with tuff T1 and AFT (Caj6, 12, 44, and 48) sample positions. (B) Corresponding formation names for the sedimentary section (Bossi, 1992) (C) Seismic sequence characteristics from the Campo Arenal, and proposed correlation to sedimentology. The seismic sequences are temporally constrained by dated tuff 2, which was collected within sequence 2 in outcrop.

TABLE 1. SEDIMENTOLOGIC DATA AND INTERPRETATIONS FOR THE EL CAJÓN SUBBASIN

Formation	Description	Interpreted environment
Tortoral Formation	Thick (up to 1 m) beds of downcutting, lenticular, boulder-rich conglomerates, and cobble-boulder sheet conglomerates with interbedded medium-grained, massive and cross-bedded sandstones.	Alluvial fan proximal deposits.
Playa del Zorro Formation	LOWER: Red-brown, fine- to medium-grained sandstones, often with vertical calcified roots preserved. Sandstones pass laterally into lenticular conglomerates and interbedded sheets of conglomerates. Rare units of root and nodule-rich sandstone. Abundant reworked mudstone and tuff clasts throughout sandstones.	Distal alluvial plain sediments with rare paleosol horizons.
	MIDDLE: Varicolored (pink, yellow, green) mudstone and muddy sandstones containing bivalves and organic matter; and thin (1–3 cm) gypsum beds. Rare red, medium-coarse-grained sandstones, planar and cross-bedded.	Lacustrine deposits. Gypsum beds and rare coarser cross-bedded sandstones indicate periodic drying-out.
	UPPER: Medium- to coarse-grained planar-bedded and cross-bedded sandstones interbedded with granular conglomerates to medium pebble tabular and lenticular conglomerates.	Alluvial plain sediments with rare paleosol horizons.
Peñas Azules Formation	Blue-gray–colored sandstones with a high proportion of basalt sand-grains and pebbles. Facies are composed of lenticular conglomerates that pass laterally into fine-grained sandstones and mudstones. Thick (up to 1 m), resistant beds of rooted sandstones and calcic preserved roots and calcareous nodules are present in thick (50 cm) beds. A thick (10–30 m) basalt unit occurs toward the top of this formation.	Ephemeral alluvial plain conglomerates and sandstones with interbedded paleosol horizons. High abundance of basaltic material probably derived from local sources to the north (Bossi, 1992).

angular unconformity. The Tortoral Formation may be equivalent to the Pliocene-Quaternary Punaschotter conglomerates that commonly cap the stratigraphy of many of the basins in the northwestern Argentine Andes (Penck, 1920; Allmendinger, 1986; Allmendinger et al., 1989; Carrapa et al., 2005).

Seismic Stratigraphy

The seismic data (see Fig. 2 for locations; Fig. 4) include 11 seismic-reflection profiles, each of which records in excess of 2 s two-way traveltime (TWTT), although the basement is commonly reached within 1.5 s TWTT. Line spacing between sections is ~5 km for dip sections, and ~12 km for strike sections; lines are between 25 and 45 km in length. In total, the seismic data cover an area of ~750 km^2. In this study, we divide the stratigraphy into four sequences (from base up: sequences 1–4), based upon standard techniques of reflector terminations, toplap and downlap surfaces, as well as seismic-reflection character (e.g., Mitchum et al., 1977; Hubbard et al., 1985a, 1985b). Previous interpretations of two of the seismic-reflection profiles (lines 01553, 10593; Cristallini et al., 2004) recognized only three sequences based upon similar criteria. In this study, we have further divided the lower sequence of Cristallini et al. (2004) into two distinct packages (sequence 1 and 2) based upon onlap relationships and unconformities present in other regions of the basin, in particular to the south.

The four sequences (Figs. 3C and 4) defined in this study occur directly above a prominent double, high-amplitude basement reflector. Sequence 1 rests conformably on basement and has a planar, continuous reflector character. Toward the top of this first sequence is a double, bright reflector. The top of this sequence is defined by a bold reflector overlain either unconformably (southern basin) or paraconformably (northern basin) by sequence 2. Sequence 2 is characterized by continuous high-amplitude reflectors in the middle of the sequence and discontinuous and variable-amplitude reflectors toward the base and top. Sequence 3 rests with a shallow-angle unconformity on the underlying sequence and is composed of dominantly discontinuous reflectors and transparent regions bounded by more-continuous, higher-amplitude, parallel reflectors. At the top of the seismic stratigraphy is sequence 4, which at times rests with an angular unconformity on sequence 3 (Fig. 4B, ii and iii) in some sections, and at others is more conformable (Fig. 4B, v). It is composed of discontinuous and continuous reflectors of variable, but most commonly high, amplitude.

Correlation of Seismic and Sedimentological Data

There is a significant spatial separation between the seismic-reflection data in the Campo del Arenal and the observed sedimentological section within the El Cajón basin. A correlation between the two data sets, therefore, should be undertaken with some care. It is, however, possible to suggest a correlation based on age data, reflector characteristics, and sedimentological observations.

The measured sedimentary sequence documents an ~1450 m section (including the Tortoral conglomerates): the seismic data record ~1500 ms TWTT. A simple conversion based crudely on 1 km of section recorded in 1 s TWTT would generate a simple comparison; however, further age and sedimentological constraints provide a more rigorous correlation. The basal contact, at 10.7 ± 1.7 Ma (Fig. 2 for location; see Sedimentary Basin Fill section), is most likely the same between the Campo del Arenal and El Cajón subbasins because sedimentation occurred on the same regionally extensive erosion surface. It is possible that there is some diachroneity to this deposition; however, this provides at least an approximate age for the base of seismic sequence 1.

The widespread unconformity between the Playa del Zorro and Tortoral Formations in the El Cajón section probably relates to the observed angular unconformity between seismic sequences 3 and 4. The discontinuous and disorganized reflector character of sequence 4 may be indicative of the cobble-boulder facies of the Tortoral Formation. Seismic sequences 1–3, therefore, correlate with the Peñas Azules and Playa del Zorro Formations. Sequence 2 is temporally constrained by the presence of a dated tuff deposited at 5.5 ± 0.9 Ma (zircon fission track; Strecker et al., 1989) at the southwestern tip of the Sierra de Quilmes (see Fig. 2 for location: seismic-reflection profile 01593; Fig. 4B, iv). Furthermore, this may be correlated to the age of 5.7 ± 0.4 Ma (Bossi et al., 2000) recorded in Playa del Zorro Formation lacustrine sediments. Seismic sequence 2, therefore, corresponds in age to the Playa del Zorro Formation, coincident with lacustrine sedimentary rocks. Sequence 1 is, therefore, probably related to the Peñas Azules Formation. The bright double reflector toward the top of seismic sequence 1 could correspond to the basalt, although this cannot be proven. The boundary between sequences 2 and 3 must be located within the coarsening-up and alluvial fan sediments of the Playa del Zorro Formation: the more pronounced alluvial sediments toward the top of the formation may correspond to the change to more disorganized and discontinuous reflector character between sequences 2 and 3. Combining these observations of sedimentary data, seismic-reflector characteristics, and temporal data generates a correlation between the El Cajón sedimentary section and the Campo del Arenal seismic sequences (Fig. 3C).

BASIN-FILL ARCHITECTURE

The primary structures of the Campo del Arenal basin have been reconstructed from the seismic sections. The basin is dominated by high-angle reverse faults dipping both to the west and east, with predominately west-dipping structures, and significantly more structures in the north than south. Many of the faults have a notable surface expression; in particular, this is true south of Sierra de Quilmes and along the reverse fault in the far northwest corner of the basin. Most of the structures follow a similar orientation to the bounding reverse fault to the west. In the following section, the timing and evolution of these structures are addressed.

A series of seismic-reflection profiles is presented here (Fig. 4) to highlight principal features within the basin. The seismic-reflection data are often of poor quality in the regions surrounding faults, where there is significant spacing between the basement reflectors; however, field data (discussed in the following) confirm the character of at least one of these structures. Commencing in the north part of the basin, the strike section 01555 exhibits a thickening and tilting of the section to the west and a reverse fault that dips to the west and offsets the basement reflectors by up to 200 ms (TWTT). Smaller faults are recognized by offsetting basement reflectors, and they often continue up into the section with little or no displacement. The upper part of the section is difficult to constrain due to the reflector quality.

Immediately to the south, section 01587 exhibits a similar tilt to the west and westward thickening. This section highlights the presence of a reverse fault that verges to the west, which does not appear to exhibit significant thickening across it, but it offsets the basement reflector by ~250 ms (TWTT). In this region of the basin, sequence 4 was either not deposited or has been completely removed by subsequent erosion.

Seismic-reflection profiles 01553 and 01593 have been previously described by Cristallini et al. (2004), who identified reverse faults dipping both west and east. These lines cross an important west-dipping reverse fault, termed the Southern Quilmes structure. Thickening occurs across this fault during sequence 2, indicating that it was active by the time sequence 1 was being deposited (Fig. 4B, iii). Downlapping

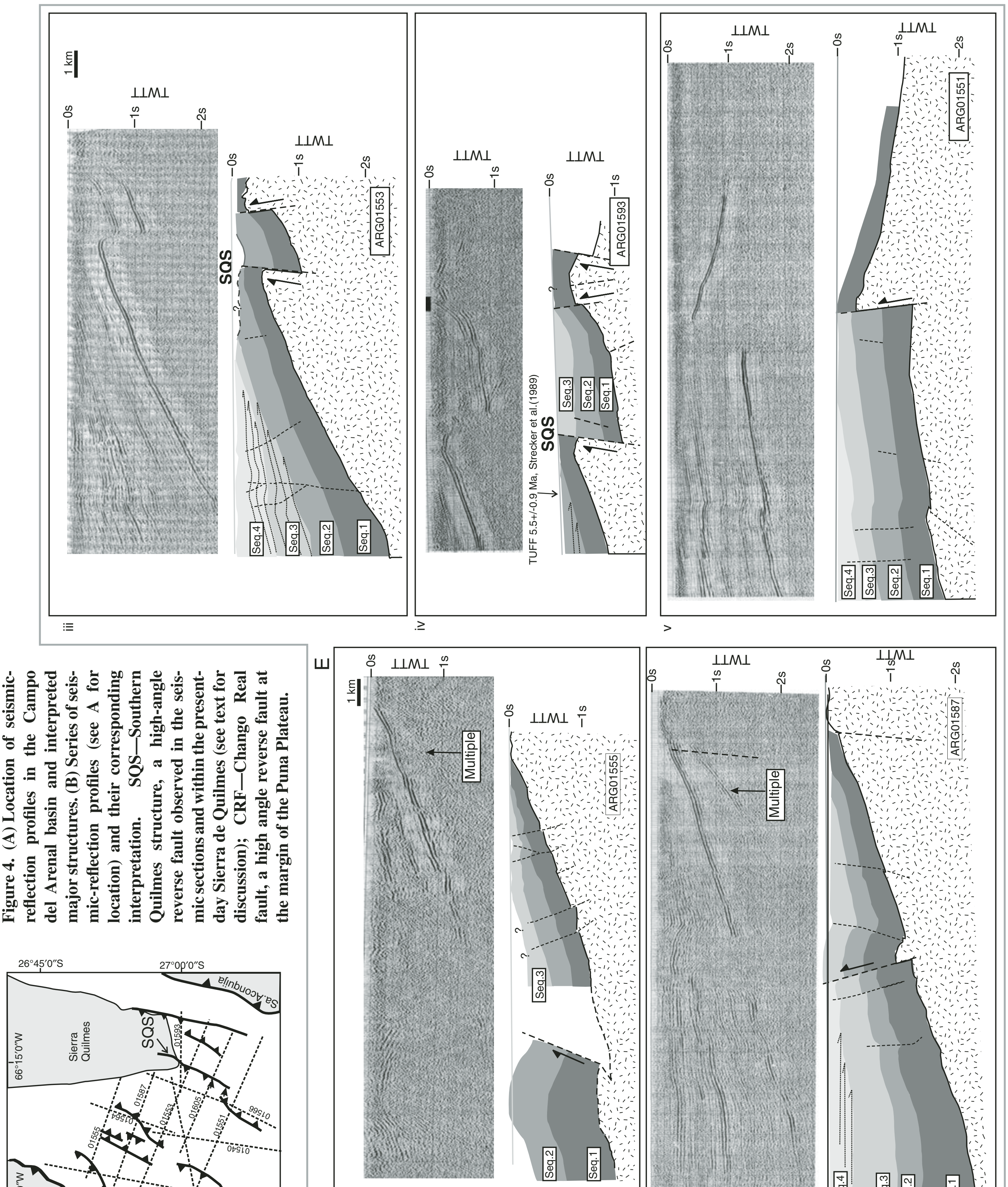

Figure 4. (A) Location of seismic-reflection profiles in the Campo del Arenal basin and interpreted major structures. (B) Series of seismic-reflection profiles (see A for location) and their corresponding interpretation. SQS—Southern Quilmes structure, a high-angle reverse fault observed in the seismic sections and within the present-day Sierra de Quilmes (see text for discussion); CRF—Chango Real fault, a high angle reverse fault at the margin of the Puna Plateau.

reflectors of sequence 3 onto 2 (Fig. 4B, iii) and sequence 2 onto 1 (Fig. 4B, iv) in the Southern Quilmes structure hanging wall further support this and indicate that activity continued through deposition of sequence 3. Vertical offset on the Southern Quilmes structure is greater than other intrabasin faults, and it reaches some 800 ms (TWTT) for the basement reflectors. Continuation of deformation along trend of the Southern Quilmes structure to the north is identified within Sierra de Quilmes where a west-dipping reverse fault has been confirmed by field observations and structural measurements. To the south, in line 01605, the Southern Quilmes structure correlates to a monocline, and onlapping reflectors and growth strata indicate its development during sequence 2.

The southernmost section, line 01551, is dominated by a west-verging reverse fault. This structure cannot be a continuation of the Southern Quilmes structure because it has both a different sense of throw, and it is separated from the Southern Quilmes structure by a monocline above which reflectors are not offset. While the full section is not preserved, there is a significant amount of displacement across this structure, with 700 ms (TWTT) of vertical offset of the basement reflector.

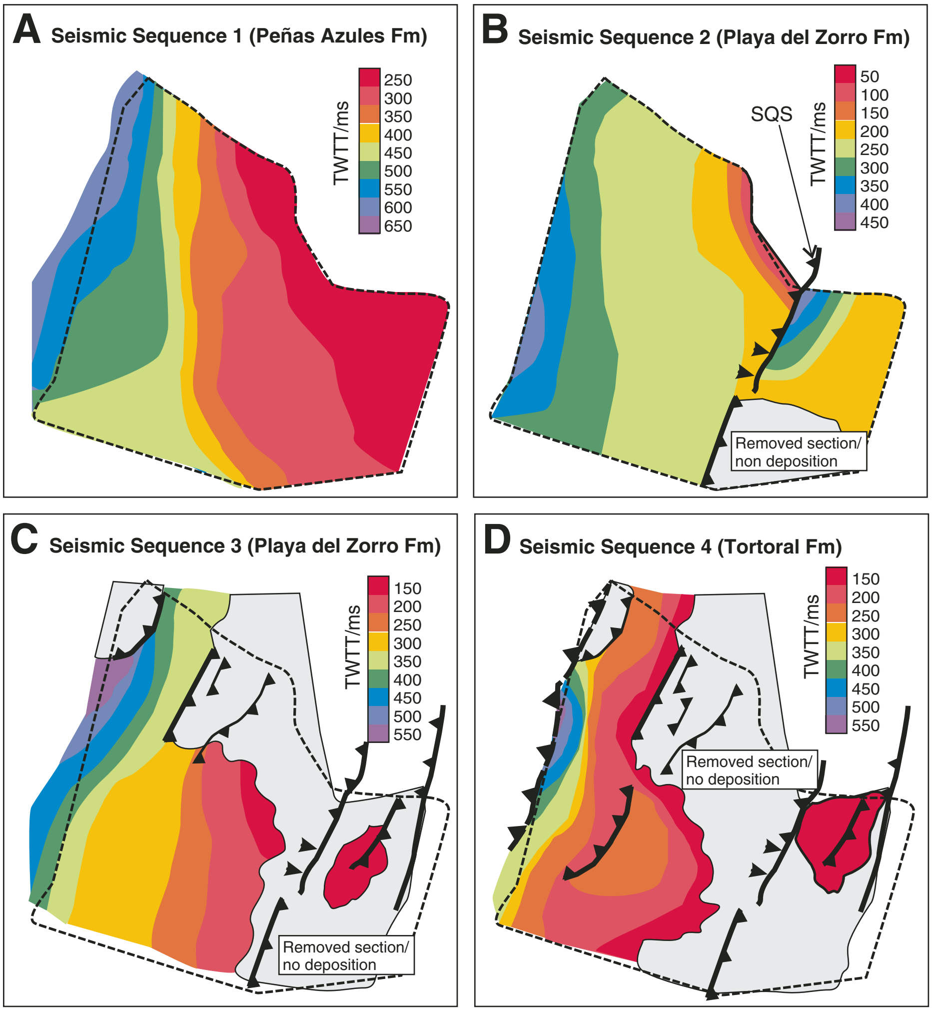

Figure 5. Isopach maps (thickness, two-way traveltime [TWTT]) for each of the four interpreted seismic sequences within the Campo del Arenal basin. (A) Sequence 1 exhibits a simple pattern of sediment thickening to the west. Deposition during this time was dominantly alluvial sediments. (B) Sequence 2 shows a similar pattern of sedimentation thickening to the west; however, sedimentation is affected by the presence of the Southern Quilmes structure (SQS). Fission-track data imply that the Sierra de Quilmes was uplifted at this time. (C) In sequence 3, sediments thicken to the west, into the Chango Real fault. It is unlikely that sediments crossed the Sierra de Quilmes at this time. Internal basin dissection due to small reverse faults occurred in the north, while the southern part of the basin was relatively undeformed. (D) During sequence 4, sediments did not cross Quilmes in the investigated area. Dissection of the basin continued in the north, and commenced in the south on small intrabasin reverse faults.

BASIN-FILL HISTORY

A series of isochron maps (Fig. 5) in ms (TWTT) has been generated through interpolation of interpreted seismic horizons. These isochron maps provide a spatial reconstruction of sedimentary depocenters and, when combined with sedimentological correlations (outlined already) and temporal constraints, they allow us to reconstruct the temporal and spatial pattern of sediment distribution and activity on intrabasin structures.

In sequence 1 (approx. Peñas Azules Formation), sediments thicken toward the west, into the basin-bounding fault (the Chango Real thrust) and, therefore, the dominant load. Sequence thickness is between 250 and 600 ms (TWTT), and the greatest thickness occurs in the northern part along the Chango Real thrust. Sedimentation at this time was dominated by alluvial fan facies. The eastward thinning of sediments occurs more abruptly in the north than south, generating a narrow-to-north and broad-to-south basin geometry. During sequence 1, no evidence of active intrabasin structures is observed in the seismic data. The thickness of sequence 1 (in excess of 250 ms TWTT) along the western margin of the Sierra de Quilmes implies that sequence 1 sediments would have been deposited over the top of it. Therefore, at this time, it is unlikely that it was affecting sediment transport.

During sequence 2 (lower-middle Playa del Zorro Formation), the overall pattern of sedimentation is similar to that of sequence 1. Sediments thicken to the west into the Chango Real thrust, although the depocenter was located farther south. Within the basin, however, significant variations in sediment thickness occur. In particular, to the south of the Sierra de Quilmes, there is thickening of sediment into the Southern Quilmes structure (up to 200 ms TWTT) and an additional fault to the south. Sedimentary facies (Fig. 3) changed from alluvial fan to lacustrine and back to alluvial facies during sequence 2. The thickness of sequence 2 along the western margin of the Sierra de Quilmes is as little as 50 ms (TWTT). This thinning toward the Sierra de Quilmes, while possibly enhanced by erosion, suggests that sediments were deposited only thinly across the range. This was possibly due to the topography being generated by this range. Much of sequence 2 has been subsequently removed by erosion in the south and east of the basin. During sequence 2, the Southern Quilmes structure and en-echelon fault to the south were the only intrabasin structures noted to affect sediment dispersal.

Sequence 3 (approx. middle to upper Playa del Zorro Formation) has experienced a significant amount of erosion, particularly where intrabasin structures have enhanced this process in the north and east. In general, sediment distribution mimics earlier sequences, thickening westward into the Chango Real thrust. Sedimentary facies during sequence 3 are coarsening-upward alluvial fan sediments. At this time, there is a notable eastward thinning of the sequence, which cannot be attributed to erosion alone. It is unlikely that sediments were deposited onto the Sierra de Quilmes, but that this range was instead a topographic feature. Exhumation of the Sierra de Quilmes might have generated the unconformity observed between sequences 2 and 3. Remnants of sequence 3 along the southern tip of the Southern Quilmes structure also suggest that it remained active, although the actual amount of displacement is difficult to ascertain due to the significant erosion. Additional variations in sediment thickness within the basin record compartmentalization of the basin into a number of smaller depocenters that occur in the northern part of the basin, in particular, along a west-dipping reverse fault in the northwest (across seismic reflections 01555 and 01538). A number of smaller faults, which exerted subtle influences on sediment distribution, also developed to the south of the Sierra de Quilmes.

Sequence 4 (Tortoral Formation) exhibits thickening of sediment toward the west, and, in particular, toward the center of the Chango Real thrust. In addition, the smaller faults in the northwest still maintained a control on sediment distribution. At this time, sedimentary facies record locally sourced alluvial fan conglomerates. The observed abrupt eastward thinning suggests that the Sierra de Quilmes was a significant topographic feature that prevented sediment transport to the east, but rather directed sediments away from this region. A significant number of small reverse faults, both west- and east-dipping, developed at this time, in particular, in the north part of the basin. Furthermore, this pattern of internal dissection propagates southward. As in sequence 3, a small package of sequence 4 remains in the Southern Quilmes structure, which is most probably the result of activity along that fault.

In summary, isochron maps coupled with sedimentary information suggest that Sierra de Quilmes was covered by alluvial fan sediments during sequence 1 and probably sequence 2; although by this time, there was a significant reduction in the amount of sediment in this region. Aside from the Southern Quilmes structure and potentially other faults within or along the present-day Sierra de Quilmes, there was no internal deformation of the basin. By sequence 3, there was a distinctive thinning to the east, and it is unlikely that material was deposited onto Sierra de Quilmes. Instead, the range was already a topographic feature. At this time, we observe dissection of the basin through out-of-sequence reverse faults in the north, and subsequently during sequence 4, the south of the basin.

APATITE FISSION-TRACK THERMOCHRONOLOGY

The AFT data from our study (Table 2) come from a basement sample that we used to determine the AFT age and exhumation history of the Sierra de Quilmes (see Fig. 2 for location). In addition, four detrital samples from a stratigraphic section (Fig. 3) through the Peñas Azules and Playa del Zorro Formations are used to investigate the evolution of the provenance history within the basin. In the vicinity of our study area, the basement ranges to the east, north, and west-southwest and the basins to the north have been studied with respect to the regional exhumation history (Coughlin et al., 1998; Coutand et al., 2001; Sobel and Strecker, 2003; Deeken et al., 2004; Carrapa et al., 2006). Therefore, we have a robust regional database for constraining potential sources.

The basement sample Caj4 is from the regional erosion surface of the Sierra de Quilmes. It was, therefore, expected to yield similar cooling histories as those obtained from the erosion surface in the adjacent Cumbres Calchaquiés Range, east of the Santa Maria valley (Sobel and Strecker, 2003). The sample has a pooled age of 81.9 ± 2.8 Ma and mean track length of 12.09 ± 0.15 µm. This sample was modeled with the AFT Solve program (Ketcham et al., 2000) (Fig. 6) using four time-temperature constraints similar to those employed by Sobel and Strecker (2003) for Cumbres Calchaquiés. The model was started at 120 Ma, with a temperature range between 80 and 160 °C, such that all tracks initially formed could be completely annealed. The shortened track-length distribution from this sample implies a late-stage heating event, consistent with the basin history suggested by the seismic data, i.e., burial of Sierra de Quilmes beneath seismic sequences 1 and 2. Modeled reheating started at 11 Ma, coincident with sedimentation in the Santa Maria basin, and the most likely timing of earliest sedimentation to occur within the El Cajón basin (minimum depositional age 10.7 ± 1.7 Ma; Strecker, 1987). At this time, the model permitted temperatures between ~15 °C and 40 °C. The age of

TABLE 2. EL CAJÓN APATITE FISSION-TRACK DATA

Sample	Irradiation code	Unit	Lat (°S)	Long (°W)	Elevation (m)	No Xls	Rho-S (x10^6)	NS	Rho-I (x10^6)	NI	P (χ^2) (%)	Rho-D (x10^6)	ND	Age (Ma)	± 1σ error	U (ppm)	Dpar (µm)	Std. Dev. (µm)	Length (µm)	Error (µm)	Std. dev. (µm)	No. lengths
Caj3	UP76-2	Granite	26°32.242′	66°22.117′	3050	19	19.0820	2091	75.3100	8253	7	1.1887	4667	55.4	1.9	79	1.96	0.09	12.28	0.17	1.82	120
Caj 4	UP57-2	Schist	26°37.540′	66°18.190′	2559	19	9.6610	665	29.1730	2008	97	1.3133	5207	81.9	2.8	28	1.81	0.14	12.09	0.15	1.51	97
Caj 48	UP57-6	Seq 4	26°39.523′	66°22.326′	2816	135	7.2220	5471	33.7380	25558	0	1.2564	8972	49.5	2.6	37	1.79	0.35	11.88	0.10	1.74	308
Caj 12	UP57-4	Seq 2	26°40.156′	66°20.225′	2575	105	4.1710	2364	33.5310	19006	0	1.2731	8972	26.8	2.5	34	1.86	0.43	11.66	0.18	1.96	122
Caj 44	UP57-5	Seq 1	26°37.558′	66°18.962′	2583	106	1.3140	1130	18.3520	15777	0	1.2647	8972	16.0	1.3	20	1.86	0.43	12.65	0.31	1.92	39
Caj 6	UP57-3	Seq 1	26°37.540′	66°18.190′	2559	90	6.1130	2580	34.4850	14555	0	1.2815	8972	44.2	3.6	33	1.70	0.27	11.18	0.17	2.03	152

Notes: Sample preparation and analysis were similar to that outlined in Sobel and Strecker (2003). Samples were analyzed with a microscope with drawing tube located above a digitizing tablet and a Kinetek computer-controlled stage driven by the FTStage program (Dumitru, 1993). Analysis was performed with reflected and transmitted light at 1250× magnification. Apatites were etched in 5.5 mol nitric acid at 20.9 °C for 20 s. Samples were irradiated at Oregon State University, USA. Following irradiation, mica external detectors were etched in 40% HF at 21.0 °C for 45 min. The pooled age (*central age*) is reported for samples with P(χ^2) greater than (*less than*) 5% as they pass (*fail*) the χ^2 test; error is one sigma, calculated using the zeta calibration method (Hurford and Green, 1983). Sample Caj 4 was counted by B. Carrapa on the Universität Potsdam Leica microscope, and ages were calculated with a zeta of 372.8 ± 5.8 (2005, personal commun.). Sample Caj3 was counted by E. Sobel at Potsdam; age was calculated with a zeta of 369.6 ± 7.6 (2005, personal commun.). Samples Caj6, 12, 44, and 48 were counted by G. Murrell on the GFZ Zeiss microscope; ages were calculated with a zeta of 348.3 ± 5.9 (2004, personal commun.).

No Xls—number of individual grains dated per sample; Rho-S—spontaneous track density; NS—number of spontaneous tracks counted; Rho-I—induced track density in external detector; NI—number of induced tracks counted; Rho-D—induced track density in external detector adjacent to CN-5 dosimetry glass; ND—number of tracks counted in determining Rho-D.

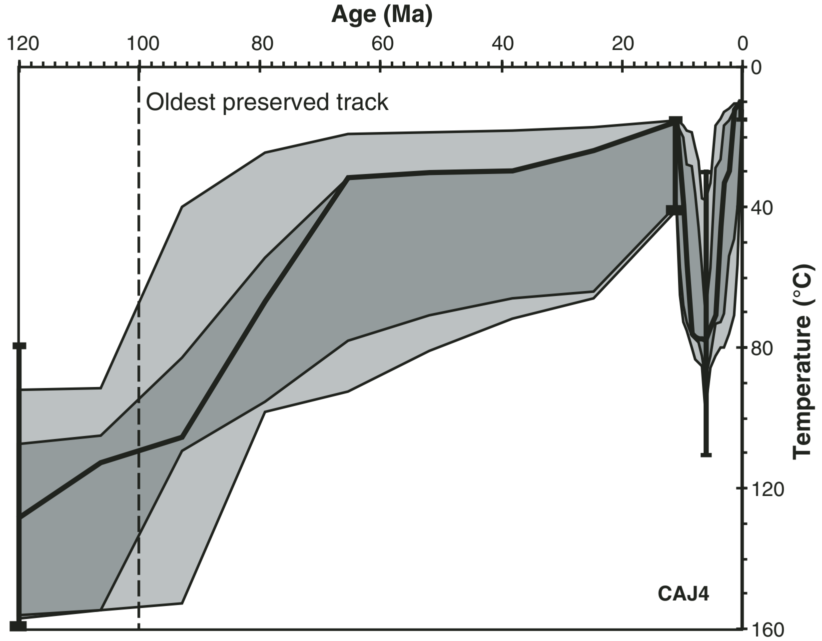

Figure 6. Apatite fission-track (AFT) age modeling results for basement sample Caj4 (see Fig. 2 for location). Best fit (dark shading) indicates burial ca. 10 Ma and subsequent exhumation ca. 6 Ma.

peak reheating was varied between 10 Ma and 5 Ma with the temperature constrained between ~30 °C and 110 °C. The final constraint was the present temperature of 10 °C to 15 °C. Heating and cooling rates were not constrained. Each model run had 10,000 iterations and 3 halvings, using a Monte Carlo approach. Note that modeling could not constrain the exact times of inflection points in the thermal history. All models yielded good fits that required reheating, consistent with the observed geological history. Modeling results (Fig. 6) are consistent with those obtained for Cumbres Calchaquiés (Sobel and Strecker, 2003) and suggest that after an initial Cretaceous cooling event, the range began to be buried during the middle Miocene, and it was finally exhumed between 9 and 5 Ma. Cretaceous cooling and formation of the erosion surface was attributed to erosion of an uplifted rift flank by Sobel and Strecker (2003), with the rift basin located east of the present Cumbres Calchaquiés.

The basement sample Caj3 is from the western margin of the northernmost El Cajón basin (northern part of the Sierra de Chango Real). This sample has a pooled age of 55.4 ± 1.9 Ma and a mean length of 12.28 ± 0.17 μm. There are few geological constraints on the exhumation history of the western flank of the basin, precluding a precise modeling strategy. Therefore we discuss only general results. AFT Solve thermal modeling suggests that the sample experienced a latest Cretaceous–early Cenozoic cooling history similar to sample Caj4. Subsequently, the sample experienced burial reheating. The younger age of Caj3 compared to Caj4 reflects either a larger amount of burial reheating and/or a later termination of the penultimate exhumation phase. Either a greater magnitude or earlier onset of burial is consistent with both model results and the position of the sample on the western flank of the basin.

For each detrital sample, fission-track grain ages (Table 2; Fig. 7) were decomposed following the binomial peak-fit method (Galbraith and Green, 1990) incorporated into the BINOFIT program (Brandon, 2002) to identify discrete populations (or component, P_0 to P_n). When plotted against depositional age, these populations define detrital (D_n) path (or trend) (Ruiz et al., 2004; Coutand et al., 2006; Fig. 8). Importantly, this type of plot also yields a graphical assessment of the lag time variability through time, thereby providing information on the long-term exhumation of the source region of a particular detrital population (Ruiz et al., 2004; Coutand et al., 2006). The youngest detrital path (D_0) is characterized by short lag times (3–4 m.y.). The abundance of apatite crystals with well-defined euhedral morphology in the P_0 population and the recurrent interbedded ashes in the stratigraphic section suggest that apatite crystals related to this path were likely derived from (reworked) ashes. The existence of the D_0 trend implies that none of the detrital samples collected in the El Cajón basin has been subjected to significant postdepositional annealing (e.g., Ruiz et al., 2004; Coutand et al., 2006). We therefore interpret all of the remaining detrital AFT ages to represent cooling events in the original source regions.

The fission-track grain ages can be subdivided into 6 D_n paths (Fig. 8; Table 3). The first, D_0, is described in the previous paragraph. The D_1 path has ages between 13.8 +7.6/–4.9 Ma and 11.2 +1.9/–1.7 Ma; and a lag time of ~7 m.y. This path first appears in sequence 2. The D_2 path is represented by a single sample in sequence 4, which has an age of 33.1 +3.2/–2.9 Ma. The D_3 path is represented by all of the samples, with ages of ca. 55 ± 5 Ma. The D_4 path also first appears in sequence 2, with ages of 83.5 +12.3/–10.7 Ma and 74.3 +9.4/–8.3 Ma. The D_5 path is represented by all samples except CAJ44 (sequence 1); it is characterized by a small number of grains with Late Jurassic to Early Cretaceous ages and large error bars (183.5 +48.9/–37.7 to 140.4 +21.5/–18.6 Ma).

Based on the fission-track data obtained from the El Cajón basin and the surrounding region, we can interpret the provenance of the D_n paths. The D_1 path must be sourced from a region where apatite crystals crossed their effective closure temperature ca. 13–11 Ma and were exposed at the surface, eroded, and first deposited into the El Cajón basin at 6 Ma (see Table 3). The average exhumation rate is given by (1) $dz/dt = [(T_c - T_s)/(dT/dz)]/\Delta t$, which is equivalent to (2) $dz/dt = Z_c/\Delta t$, where T_c is the closure temperature, T_s is the surface temperature, dT/dz is the geothermal gradient, Δt is the lag time, and Z_c is the closure depth. For a lag time Δt = 7 m.y., T_c = 110° ± 5 °C, T_s = 15 °C, dT/dz = 25 ± 5 °C, and Equations 1 and 2 yield a range of exhumation rates of 0.4–0.7 mm/yr; at least between 13 and 3 Ma for the source region of the P_1 detrital population. The source area of this population is, to date, unknown: either it is a range that was exhumed rapidly but has not yet been dated; or it is a Miocene volcanic center, as yet unidentified. The latter is unlikely given that the lag time is approximately constant and not increasing (an increasing lag time would be anticipated for a single-age volcanic body source being eroded).

The D_2 path could possibly have been derived from Sierra de Chango Real, which yielded AFT ages between 38 and 29 Ma indicative of rapid cooling (Coutand et al., 2002), located to the west-southwest and along the margin of the Puna. The D_3 path is associated with a broad span of very consistent ages. This pattern could be derived from the exhumation of an exhumed partial annealing zone that would have been formerly widely exposed to the north-northwest (Deeken et al., 2004; Coutand et al., 2006). Alternatively, the source could be the region

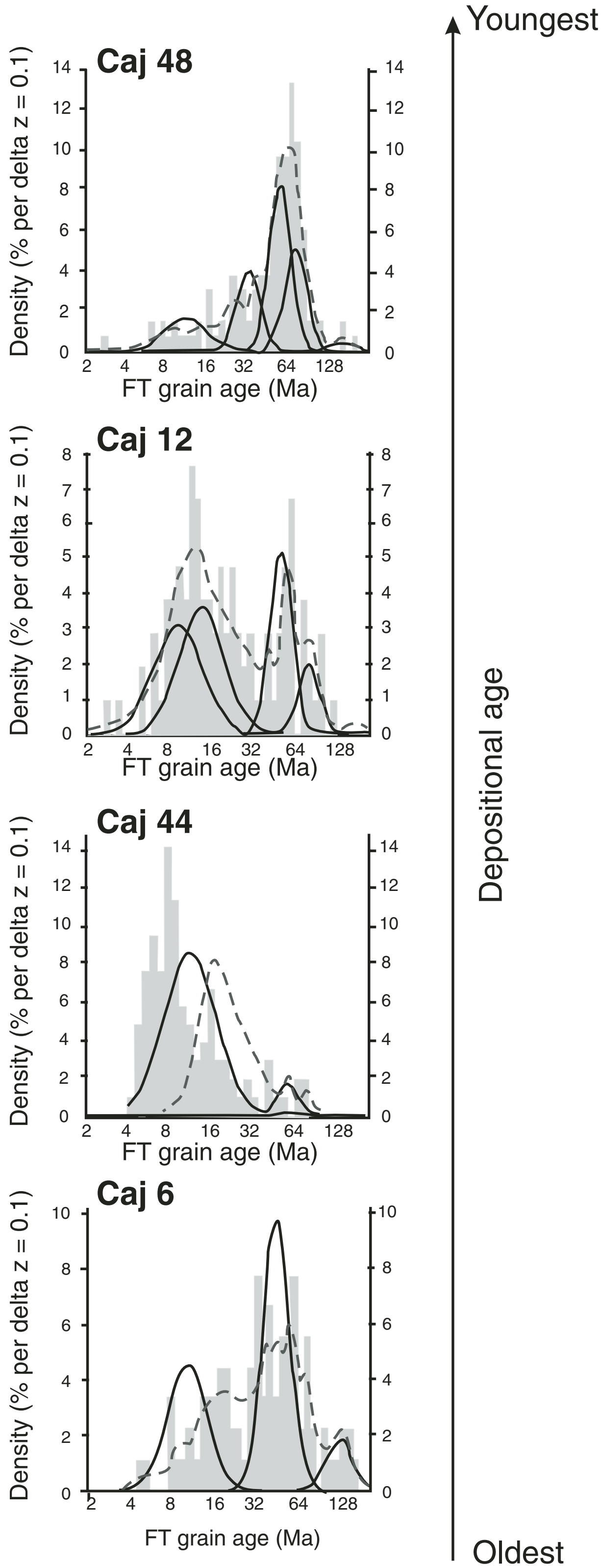

Figure 7. Plot of probability density (histogram) and probability density function (dashed line) of age distribution of each detrital sample. Fission-track (FT) grain age populations are shown by solid black lines.

TABLE 3. APATITE FISSION-TRACK GRAIN AGE DISTRIBUTIONS

			D_0			D_1			D_2			D_3			D_4			D_5		
Sample	Seq.	Dep. age	P_1 (%)	−Error	+Error	P_2 (%)	−Error	+Error	P_3 (%)	−Error	+Error	P_4 (%)	−Error	+Error	P_5 (%)	−Error	+Error	P_6 (%)	−Error	+Error
CAJ48	3	3				11.2 (14.3)	1.7	1.9	33.1 (20.0)	2.9	3.2	56.5 (39.3)	5.3	5.9	74.3 (24.2)	8.3	9.4	162.1 (2.2)	37.7	48.9
CAJ12	2	6	9.2 (31.6)	2.4	3.3	13.8 (34.2)	4.9	7.6				51.7 (24.0)	4.2	4.6	83.5 (9.4)	10.7	12.3	183.5 (0.8)	88.1	167.2
CAJ44	1	8	11.4 (92.9)	0.9	1.0							59.0 (7.1)	6.7	7.5						
CAJ6	1	10.5	14.6 (37.0)	1.5	1.7							53.9 (53.2)	3.6	3.9				140.4 (9.8)	18.6	21.5

†All errors are ±95% confidence interval, and all ages given are in Ma (depositional ages are approximate).

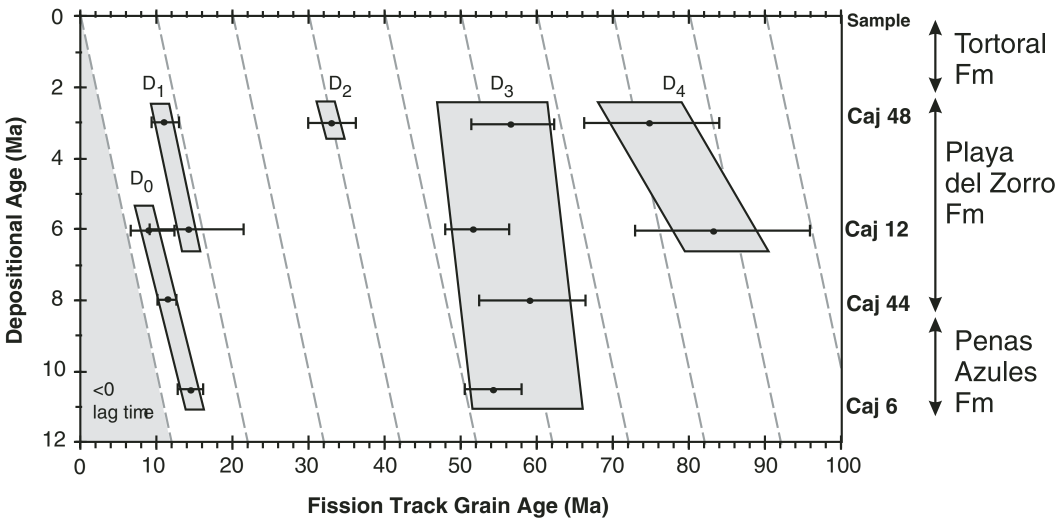

Figure 8. Plot of depositional age versus apatite fission-track (AFT) grain age for the detrital AFT samples within the El Cajón basin. Samples are indicated with approximate depositional age. Five AFT age populations are recognized (D_1–D_4). Not shown is D_5, which is composed of three AFT grain ages of ca. 150 Ma with large errors. This population is not present in Caj 44. Population D_4 has ages typical of the regional basement erosion surface, and that of AFT basement sample Caj 4 (taken from the basement erosion surface of the Sierra de Quilmes).

on the NW flank of the El Cajón basin, where sample Caj3 yields an identical age. The D_4 path, which appears above sequence 1, has ages that are typical of the regional erosion surface exposed in the Sierra de Quilmes (e.g., basement sample Caj4). The small number of old grains represented by the D_5 path could either be recycled detrital apatite or could be derived from regions with very little exhumation, such as the Puna Plateau, or from the northernmost extent of the Precordillera and Sierras Pampeanas ranges to the southwest, which are characterized by Jurassic and Early Cretaceous ages (Coughlin et al., 1998; Deeken et al., 2004). The simultaneous appearance of the D_1 and D_4 paths suggests that a basin-drainage reorganization occurred between sequences 1 and 2. Furthermore, we hypothesize that the appearance of the D_4 path marks the onset of erosion and uplift of the basement surface of the northern Sierra de Quilmes at this time in the northern El Cajón basin. Hence, by this time, the overlying sediment had been removed.

The combination of geological and detrital AFT data implies that derivation of detritus from the Sierra de Quilmes in the northern El Cajón basin had commenced by 6 Ma. Thermal modeling of the basement AFT sample from this range requires a reheating during the middle Miocene and subsequent re-exhumation between 9 and 5 Ma. The reheating is most simply explained by burial beneath sediments overlying the range, beginning at the onset of sedimentation into the El Cajón–Campo del Arenal basin by ca. 11 Ma. The subsequent exhumation must have commenced prior to 6 Ma, because we record detrital grains being eroded and supplied from this range at this time, implying that the sedimentary cover had already been removed. Prior to 6 Ma, we do not record detrital grains derived from the range. We therefore infer the uplift and exhumation of at least the northern Sierra de Quilmes prior to 7–6 Ma. In fact, Butz et al. (1995) and Deeken et al. (2006) have demonstrated that the exhumation at Cerro Durazno, a range immediately to the north and transitional with Sierra de Quilmes, began exhumation between 12 and 7 Ma.

BASIN EVOLUTION

We propose a model of basin evolution for the past 11 Ma (Fig. 9) that combines the seismic, sedimentologic, and temporal data and integrates this with new basement and detrital AFT age data. During deposition of the Peñas Azules Formation (ca. 11–6 Ma; middle–late Miocene; seismic sequence 1), the basin was strongly influenced by loading to the west along the Chango Real thrust. This created a simple pattern of sedimentation with deposition focused along the Chango Real thrust and thinning to the east across the El Cajón–Campo del Arenal, and most likely across into the Santa Maria basin, which may at this time have been connected to the El Cajón–Campo del Arenal basin (Bossi, 1992). In turn, at this time, the Santa Maria basin may have been contiguous with the basin on the eastern flank of the Sierra de Aconquija (Sobel and Strecker, 2003).

During the late Miocene to early Pliocene (younger than 6 Ma; sequence 2; lower Playa del Zorro Formation), intrabasin deformation began. Sedimentation in the southern part of the basin was affected by a number of faults located to the south and within the present-day Sierra de Quilmes. Exhumation of the Sierra de Quilmes may have begun at this time, in the north; however, sediments still crossed between the Campo del Arenal and Santa Maria basin across the structure in the south. AFT age modeling of a basement sample (Caj4) from the Sierra de Quilmes, as well as the first occurrence of the D_4 path in the detritic fraction of sequence 2, supports this timing for exhumation of the range. The (AFT) model indicates burial starting in mid-Miocene time, and re-exhumation commencing prior to ca. 6–5 Ma. Furthermore, detrital samples from the El Cajón subbasin first record grains derived from a source consistent with the Sierra de Quilmes at ca. 6 Ma. For most of this time, sedimentation was dominantly of alluvial plain sediments; however, between ca. 6 and 5 Ma, lacustrine sediments were deposited.

By the time of deposition of the upper Playa del Zorro Formation (middle Pliocene; sequence 3), the Sierra de Quilmes was a distinctive feature in the south that separated the El Cajón and northern Campo del Arenal basins from the Santa Maria basin. Sequences 1 and 2 sediments were most likely folded and subsequently eroded from the range. Furthermore, at this time, the north part of the basin experienced increased shortening as small, out-of-sequence thrusts dissected the internal fill and the basin was compressed between the Sierra de Quilmes and the propagating Chango Real thrust. Sedimentation was dominated by alluvial fan sediments. These were derived not only from the west from the Chango Real thrust, but also, as AFT grain age data suggest, from the east, i.e., Sierra de Quilmes.

During sequence 4, the basin was further dissected, and it shortened progressively from north to south, generating the present-day "A"-shaped geometry. This progressive migration of internal fragmentation from north to south could be related to a north-south propagation of exhumation of the Sierra de Quilmes. In this model, the Southern Quilmes structure has been entrained and uplifted into the present-day Sierra de Quilmes.

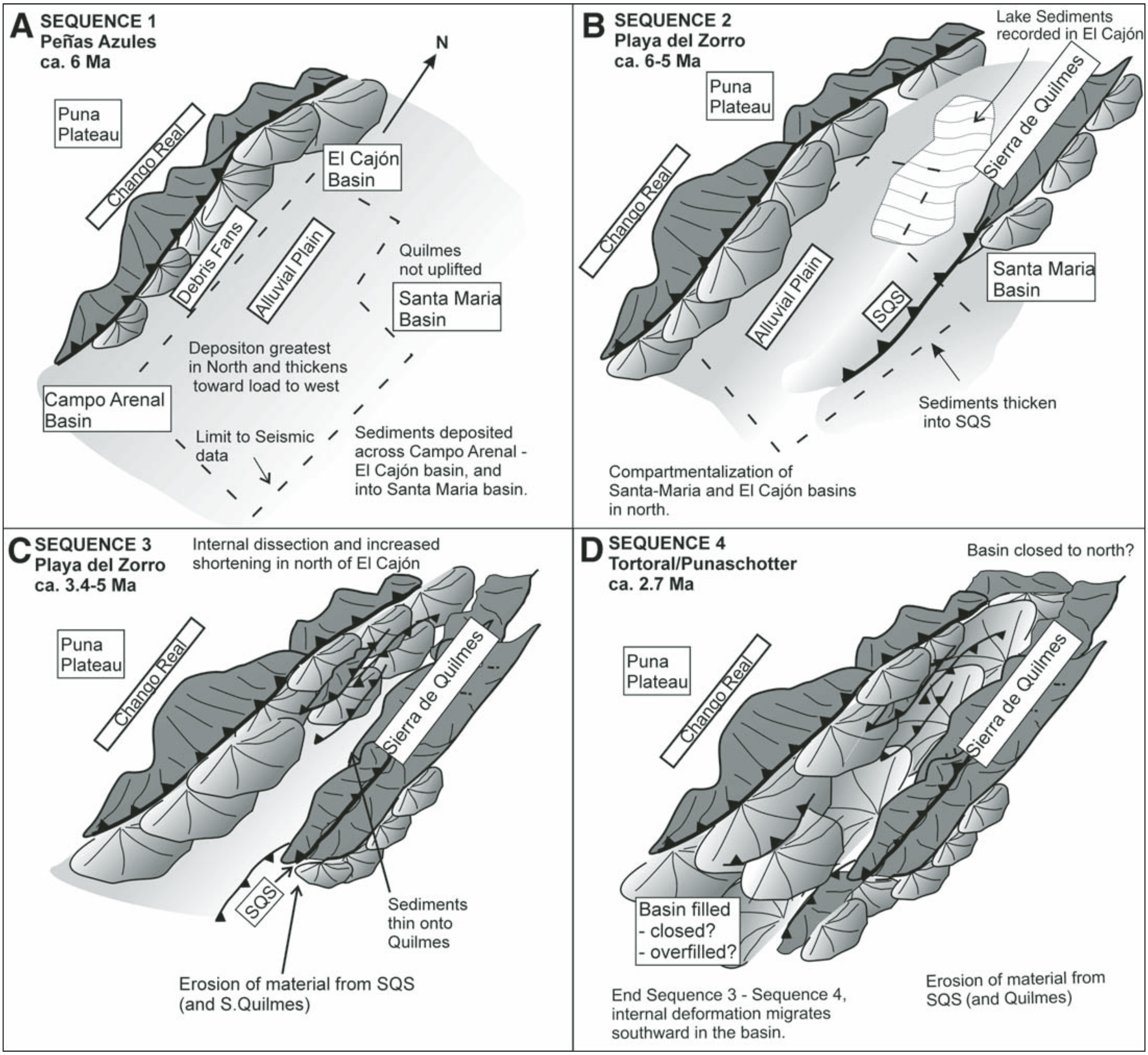

Figure 9. Proposed fragmentation of the foreland produced by the out-of-sequence basement uplift of the Sierra de Quilmes. The Sierra de Quilmes uplift commenced in the north and propagated south, while deformation in the El Cajón–Campo del Arenal (EC-CA) basin was accommodated onto small intrabasin reverse faults due to the shortening between the Sierra de Chango Real and the Sierra de Quilmes. Sequence 1: sediments were deposited into the accommodation space created by the load of the Sierra de Chango Real to the west of the El Cajón–Campo del Arenal basin. Sierra de Aconquija were probably uplifting (covered in sediments) just prior to 6 Ma. Sequence 2: The Sierra de Aconquija were uplifted along a high-angle east-dipping reverse fault while being stripped of sediment. Uplift of the Sierra de Quilmes occurred out-of-sequence, either due to the load at both basin margins or slowing of uplift of the Sierra de Aconquija as basement rocks were eroded. The Sierra de Quilmes separated the El Cajón–Campo del Arenal basin from the Santa Maria basin. Further fragmentation and sediment accumulation continued to the south with activity on the Southern Quilmes structure (SQS). Lacustrine sediments were deposited into the basin. Sequence 3: Sediments were eroded off the Sierra de Quilmes as it is uplifted in the south. In the northern part of El Cajón–Campo del Arenal, the basin was further fragmented by smaller intrabasin reverse faults as the basin was compressed between Sierra de Chango Real and the Sierra de Quilmes. Sequence 4: uplift of Sierra Quilmes propagated south, resulting in El Cajón–Campo del Arenal basin narrowing from north to south. Internal dissection of basin propagated south as compression between bounding ranges extended southward. Fanglomerates were deposited across entire region, and the narrow basin was filled, either by overfilling (transport limited) or due to complete closure.

The evolution of the basin, therefore, is characterized by a simple pattern of basin filling first complicated by exhumation of Sierra de Quilmes and later by intrabasin faulting. The sedimentary fill of the basin is, generally, a coarsening-up succession, aside from an interval of lacustrine deposition during the initial uplift of the Sierra de Quilmes. Progressive coarsening of the facies is probably related to the source region becoming more proximal as the basin narrowed from the north. The presence of lacustrine sediments in the El Cajón basin is coeval with lacustrine sediments recorded in the Santa Maria basin ca. 6 Ma (Bossi et al., 2000).

DISCUSSION

Our data record a pattern of basin compartmentalization and fragmentation. First, uplift of the Sierra de Quilmes at ca. 6 Ma separated the El Cajón–Campo del Arenal basin from the foreland; second, through continued shortening, further intrabasin structures fragmented the El Cajón basin progressively from north to south as it was deformed between the Sierra del Chango Real and the Sierra de Quilmes. This migration of deformation southward within the basin was possibly associated with the implied southward progression of uplift of the Sierra de Quilmes. In the following, we first consider the mechanism for uplift of the Sierra de Quilmes before this is then integrated with our current understanding of the development of foreland regions. We also propose a hypothesis for the evolution and incorporation of the El Cajón–Campo del Arenal basin into the orogen and its separation from the foreland through fragmentation of a previously contiguous foreland. It is proposed that this occurred as deformation was accommodated between different basement uplifts, either along high-angle reverse faults or basement flexures. In addition, the role of preexisting structures, i.e., the superimposition of this region onto the Salta Rift, is examined in the timing and pattern of basement uplift, and the importance of this structural superimposition is highlighted in the style and timing of fragmentation and internal basin deformation.

First, we consider the Sierra de Quilmes, which was uplifted and providing a source of sediment into the basin by ca. 6 Ma. The geometry of the basin (narrow in the north and wide in the south), the pattern of sedimentation, and timing of intrabasin structures (younger in south) suggest that this uplift is likely to have occurred diachronously along strike, which is in agreement with inferred earlier uplift of the northern continuation of Sierra de Quilmes (Butz et al., 1995). The timing of uplift in the southern sector is also coincident with or shortly subsequent to that of the Sierra de Aconquija, which forms the bounding range of the Santa Maria basin to the east (Bossi, 1992; Sobel and Strecker, 2003). The location of the uplifting Sierra de Quilmes is almost exactly centrally positioned between the Sierra de Aconquija to the east, and the Sierra del Chango Real to the west. A propagation of reverse faulting into the foreland is one mechanism proposed for the incorporation of former foreland basins as intervening basins that are bounded by basement uplifts that surround the Puna Plateau (e.g., Strecker et al., 1989; Allmendinger et al., 1997; Coughlin et al., 1998; Hilley and Strecker, 2005), and characterize the Sierras Pampeanas. The increasing degree of the tectonic load, and increasing proximity of basement ranges of the eastern margin of the Puna Plateau could account for the upward coarsening recorded in sediments during sequence 1. The mechanism for the propagation of uplifts into the marginal areas may possibly be explained by an increase in lithostatic stresses in the plateau (Sobel et al., 2003; Hilley and Strecker, 2005). In this respect, the inferred mantle delamination in the present-day Puna-Altiplano region (e.g., Kay et al., 1994) and ensuing wholesale isostatic plateau uplift (Garzione et al., 2006) that followed an earlier phase of distributed shortening and uplift may indeed have triggered the younger uplifts in the northern Sierra de Pampeanas. However, regardless of the mechanism driving the propagation of deformation into the foreland, the uplift of the Sierras Aconquija generated a load along the eastern margin of the basin and thickening of sediments in the Santa Maria basin (Bossi, 1992; de Urreiztieta, 1996).

The Sierra de Quilmes is not uplifted along a reverse fault (although farther north, we cannot constrain if it is underpinned by a structure), but rather it is a complicated uplift (anticline) that has several reverse faults both within it and along its southeastern margin (this study; Cristallini et al., 2004). The close temporal relationship between uplift of the Sierra de Aconquija and later the Sierra de Quilmes raises the possibility that this east-dipping fault (bounding the Sierra de Aconquija) somehow affected deformation within the El Cajón–Campo del Arenal basin, either by preventing deformation from propagating east or by producing sufficient loading at the margins to create flexure and deformation within the basin. This might explain the fixed position of this range in approximately the center of the basin. An alternative hypothesis that might explain an intrabasin uplift is that uplift of the Sierra de Aconquija was slowed (i.e., displacement on the fault slowed) once the sediment had been stripped from the range and the basement rocks exposed (thus erosion rate lowered) as proposed by Sobel and Strecker (2003). In this scenario, shortening was then accommodated within the basin, while deformation could not propagate east into the foreland. The observed propagation of shortening and deformation from north to south most likely relates to the obliquity of the Sierra de Quilmes to the Sierra de Chango Real and the Sierra de Aconquija.

We hypothesize that the mechanism for observed out-of-sequence basement uplift and continued style of deformation within the basin is fundamentally related to the reactivation of the fault bounding the Sierra de Aconquija, whether through the generation of a double load and flexure or displacement slowing and prevention of deformation propagation into the foreland. The most likely explanation for the architecture of this fault relates to the superimposition of the deformation onto the Salta Rift province. The combination of horizontal stresses (e.g., Jordan et al., 1983; Alvarado and Beck, 2006) and these preexisting zones of weakness in the Sierras de Pampeanas (e.g., Mon and Salfity, 1995; Schmidt et al., 1995; Ramos et al., 2002; Cristallini et al., 2004) and the neighboring Eastern Cordillera (Allmendinger et al., 1983; Grier et al., 1991; Hongn and Seggiaro, 2001) has favored the widely distributed reactivation of extensional structures.

AFT data from the Cumbres Calchaquiés Range to the northeast document a Cretaceous cooling event that is interpreted to have been driven by rift-flank uplift (Bossi, 1992; Sobel and Strecker, 2003) associated with rifting, as a southern extension of the Salta Rift or associated rifting at that time. This is similar to other basin-bounding structures, such as the margin of the Famatina basin to the south (Davila and Astini, 2003), the Sierra de Luracatao located to the north (Hongn and Seggiaro, 2001; Deeken et al., 2006), and other ranges in the transition between the Sierras Pampeanas and the Eastern Cordillera (Grier et al., 1991). It is, therefore, highly likely that structures associated with the Salta Rift have been utilized in compression in this region of the Sierras Pampeanas. More specifically, the east-dipping reverse fault that bounds the western margin of Sierra de Aconquija is likely the result of structural inversion of a previous fault. Our data, therefore, highlight the importance of activation of the extensional N-NW to S-SE structural trend but do not suggest reactivation of NE-SW structures of the inferred Tucumán lineament (e.g., Mon, 1979; de Urreiztieta, 1996). This is possibly related to the orientation of structures relative to shortening.

The overall style of fragmentation observed in the Sierras Pampeanas might be anticipated in other thick-skinned regions with similar structural heterogeneity. In an analogous situation in the Laramide province, it has been inferred that normal faults have been reactivated in compression and linked to the evolution of the basement uplifts (Schmidt and Garihan, 1983; Marshak et al., 2000; Bump, 2003). In another example of a thick-skinned foreland, an out-of-sequence intrabasin basement uplift is observed at the Gory Baybeiche Range within the Kyrgyz Central Tien Shan (Burbank et al., 1999). Although there is no evidence for structural reactivation of this uplift, the older Atbashy range, to the south, is localized by a late Paleozoic suture (Khristov and Mikolaychuk, 1983).

The uplift of the Sierra de Quilmes was coincident with the deposition of lacustrine units in the El Cajón basin (Bossi, 1992). The occurrence of lacustrine sediments at this time could be (1) related to a more humid climate and/or (2) due to a reorganization of drainage associated with the uplift of the range as the system readjusted to a change in tectonic setting. Lake sediments have been recorded in other similar tectonic settings where thick-skinned basement uplifts fragment the foreland, such as in the Wind River basin (Phillips, 1983; Steidtmann et al., 1983); and in the Green River Formation of Wyoming, uplift of basement ranges generated a reorganization of basin drainage that led to the development of lacustrine sediments due to sediment starvation once the range had been stripped of sediment (Carroll et al., 2006).

Here, uplift of the Sierra Quilmes, which occurred out of sequence within the basin, is proposed to have occurred due to the effect of a double load. Firstly, the presence of the reverse fault bounding the Sierra de Aconquija prevented the load and deformation from propagating out into the foreland, while the load generated by the Sierra de Chango Real remained on the western margin of the basin, and shortening continued. It is at this time, during the deposition of sequence 2, that the El Cajón–Campo del Arenal basin may have become integrated into the orogen and been uplifted together with the Sierra Quilmes basement block. This effective trapping of the basin between these two ranges, and the fixed location of the uplifting Sierra de Quilmes had significant implications for the internal deformation within the El Cajón–Campo del Arenal basin, which was then being compressed between the Sierra de Chango Real and, progressively along the western margin, the uplifting Sierra de Quilmes. This led to further out-of-sequence faulting within the basin, and deformation progressed from the north to the south within the El Cajón basin. The continued shortening and progressive uplift of Sierra de Quilmes from north to south generated reverse faults with greater displacement in the north part of the basin than the south.

This pattern of basin shortening and internal basin dissection and uplift apparently prevailed throughout sequence 3 as the section continued to coarsen and the basin filled. Sequence 4 marks a significant change in facies regime (significantly more coarse-grained), and basin filling to high levels (Strecker, 1987). This change could have been related to increased sediment supply and overfilling, either with or alternatively due to a change in climate. This pattern of basin filling was not, however, maintained, and the El Cajón–Campo del Arenal basin was excavated during the Quaternary. This pattern of basin fragmentation associated with lacustrine and subsequent filling is exemplified by the fluvio-lacustrine units of the Wind River basin of Wyoming (Phillips, 1983; Steidtmann et al., 1983). It is not clear whether internal draining of these basins occurred throughout their history or if it was transient, or whether sediment supply was too great for the transport (transport limited) and thus the basins filled. Regardless, in the Wind River basin of the U.S. (e.g., Flanagan and Montagne, 1993), the El Cajón basin, and numerous other basins in northwestern Argentina (e.g., Hilley and Strecker, 2005; Strecker et al., 2007), these basin fills were subsequently excavated and the basins were fully reintegrated with foreland drainage systems.

In summary, the El Cajón–Campo del Arenal basin exhibits characteristics in its development that are typical of a broken foreland region, and reflect the interactions between the topographic evolution of uplifting areas and neighboring preexisting structures predicted by Hilley et al. (2005). The reactivation of a previously extensional structure that bounds the present-day Sierra de Aconquija generated the fragmentation of the foreland through the out-of-sequence uplift of the Sierra de Quilmes and inclusion of the El Cajón–Campo del Arenal basin into the orogenic realm. Similar to many of the features observed within the thick-skinned region of the Laramide orogen, it highlights the potential for the reactivation of preexisting structures to localize deformation in the basin. The El Cajón–Campo del Arenal basin evidence enables us to propose a mechanism for out-of-sequence intrabasin basement uplifts that do not themselves require preexisting structures. There is, therefore, opportunity for fragmentation due to reactivation of structures in regions, such as the Qilian Shan of north-western China, where structural reactivation is documented, but there is an absence of chronological data.

CONCLUSIONS

The El Cajón–Campo del Arenal basin evolved from an undisturbed foreland into a fragmented region due to an out-of-sequence basement uplift that occurred ca. 6 Ma. This intrabasin flexure was caused by the uplift of the Sierra de Aconquija to the east by means of reactivation of a previously extensional structure in compression. This west-dipping reverse fault coupled with the existing east-dipping fault that bounds the Sierra del Chango Real generated a double load on the basin The immobility of this intrabasin range led to further deformation and out-of-sequence thrusting as the El Cajón–Campo Arenal basin was shortened between the two ranges.

The role of preexisting structures in this basin highlights their importance in other examples of thick-skinned foreland basins with existing basement structure. In these regions, there is not a self-similar style of propagation into the foreland but rather one that utilizes additional structures to enhance the uplift and incorporation of basins into the orogen, which may exhibit a degree of randomness in the spatio-temporal uplift of ranges.

ACKNOWLEDGMENTS

We are grateful for financial support by the German Science Foundation (DFG) through funds of the Leibniz grant to M. Strecker. B. Carrapa, I. Coutand, and L. Schoenbohm were supported by the Alexander von Humboldt foundation. Our thanks are extended to G. Murrell for dating detrital apatite fission-track samples; G. Hilley, A. Villanueva, and U. Strecker for fruitful discussions; and B. Fabian for help with artwork. We thank P. DeCelles, J. Schmitt, and associate editor D. Lageson for thorough reviews of an earlier version of this paper. We thank ANDES, SA, Argentina, for access to and permission to publish seismic sections. M. Strecker also acknowledges the A. Cox Fund of Stanford University for additional support.

REFERENCES CITED

Allmendinger, R., 1986, Tectonic development, southeastern border of the Puna Plateau, north-western Argentine Andes: Geological Society of America Bulletin, v. 97, p. 1070–1082, doi: 10.1130/0016-7606(1986)97<1070:TDSBOT>2.0.CO;2.

Allmendinger, R., Ramos, V.A., Jordan, T.E., Palma, M., and Isacks, B.L., 1983, Paleogeography and Andean structural geometry, northwest Argentina: Tectonics, v. 2, p. 1–16.

Allmendinger, R., Strecker, M.R., Ermchuck, M., and Francis, P., 1989, Neotectonic deformation of the southern Puna Plateau, north-western Argentina: Journal of South American Earth Sciences, v. 2, p. 111–130, doi: 10.1016/0895-9811(89)90040-0.

Allmendinger, R., Jordan, T., Kay, S., and Isacks, B., 1997, The evolution of the Altiplano–Puna Plateau of the Central Andes: Annual Reviews of Earth and Planetary Science Letters, v. 25, p. 139–174.

Alvarado, P., and Beck, S., 2006, Source characterization of the San Juan (Argentina) crustal earthquakes of 15 January 1944 (M_w7.0) and 11 June 1952 (M_w6.8): Earth and Planetary Science Letters, v. 243, p. 615–631.

Bossi, G.E., 1992, Historia de subsidencia del perfil tipo del Neogeno del Valle de Santa Maria: IV Reunion Argentina de Sedimentologia, v. 1, p. 155–172.

Bossi, G.E., Muruaga, C., Georgieff, S.M., Ahumada, A.L., Ibanez, L.M., and Vides, M.E., 1997, The Santa Maria–Hualfin Neogene basin of the Pampean Ranges: An example of mixed tectonic evolution: Porlamar, Venezuela, Congresso Latino Americano de Sedimentologia, v. 4, p. 97–104.

Bossi, G.E., Vides, M.E., Ahumada, A.L., Georgieff, S.M., Muruaga, C., and Ibanez, L.M., 2000, Analisis de las paleocorrientes y de la varianza de los componentes a tres niveles, Neogeno del Valle del Cajón, Catamarca, Argentina: Asociación Argentina de Sedimentología Revista, v. 7, p. 23–47.

Brandon, M.T., 2002, Decomposition of mixed age distributions using Binomfit: On track: Newsletter of the International Fission Track Community, v. 24, p. 13–18.

Bump, A., 2003, Reactivation, trishear modelling, and folded basement in Laramide uplifts: Implications for the origins of intra-continental faults: GSA Today, v. 13, no. 3, p. 4–10, doi: 10.1130/1052-5173(2003)013<0004:RTMAFB>2.0.CO;2.

Burbank, D.W., McLean, J.K., Bullen, M., Abdrakhmatov, K.Y., and Miller, M.M., 1999, Partitioning of intermontane basins by thrust-related folding, Tien Shan, Kyrgyzstan: Basin Research, v. 11, p. 75–92, doi: 10.1046/j.1365-2117.1999.00086.x.

Burtman, V.S., 1975, Structural geology of the Variscan Tien Shan: American Journal of Science, v. 280, p. 725–744.

Butz, D.J., Foldesi, C.P., and Reynolds, J.H., 1995, Provenance of the Payogastilla Group: A preliminary uplift history of the Central Andes, Salta Province, NW Argentina: GSA Abstracts with Programs, v. 27, no. 2, p. 39.

Caminos, R., 1979, Sierras Pampeanas noroccidentales, Salta, Tucuman, Catamarca, La Rioja Y San Juan, *in* Castellanos, T.G., ed., II Simposio Geologia Regional Argentina: Córdoba, Academia nacional de Ciencias, p. 225–291.

Carrapa, B., Wijbrans, J., and Bertotti, G., 2004, Detecting provenance variations and cooling patterns within the Western Alpine orogen through ^{40}Ar/^{39}Ar geochronology on detrital sediments: The Tertiary Piedmont Basin, NW Italy, *in* Matthias, B., and Spiegel, C., eds., Detrital Thermochronology—Provenance Analysis, Exhumation, and Landscape Evolution of Mountain Belts: Geological Society of America Special Paper 378, p. 67–103.

Carrapa, B., Adelmann, D., Hilley, G., Mortimer, E., Sobel, E., and Strecker, M., 2005, Oligocene uplift, establishment of internal drainage and development of plateau morphology in the southern Central Andes: Tectonics, v. 24, p. 210–234.

Carroll, A.R., Chetel, L.M., and Elliot Smith, M., 2006, Feast to famine: Sediment supply control on Laramide basin fill: Geology, v. 34, p. 197–200, doi: 10.1130/G22148.1.

Cerveny, P.F., Naeser, N.D., Zeitler, P.K., Naeser, C.W., and Johnson, N.M., 1988, History of uplift and relief of the Himalaya during the past 18 million years: Evidence from fission-track ages of detrital zircons from sandstones of the Siwalik Group, *in* Kleinspehn, K.L., and Paola, C., eds., New Perspectives in Basin Analysis: New York, Springer, p. 43–61.

Coughlin, T.J., O'Sullivan, P.B., Kohn, B.P., and Rodney, J.H., 1998, Apatite fission-track thermochronology of the Sierras Pampeanas, central western Argentina: Implications for the mechanism of plateau uplift in the Andes: Geology, v. 26, no. 11, p. 999–1002, doi: 10.1130/0091-7613(1998)026<0999:AFTTOT>2.3.CO;2.

Coutand, I., Cobbold, P.R., de Urreiztieta, M., Gautier, P., Chauvin, A., Gapais, D., Rossello, E.A., and Lòpez-Gamundí, O., 2001, Style and history of Andean deformation, Puna Plateau, north-western Argentina: Tectonics, v. 20, p. 210–234, doi: 10.1029/2000TC900031.

Coutand, I., Strecker, M.R., Thiede, R., Arrowsmith, J.R., Hilley, G.E., Korjenkov, A., and Omuraliev, M., 2002, Late Cenozoic tectonic development of the intramontane Alai Valley, (Pamir-Tien Shan region, central Asia): An example of intracontinental deformation due to the Indo-Eurasia collision: Tectonics, v. 21, p. 1053, doi: 10.1029/2002TC001358.

Coutand, I., Carrapa, B., Deeken, A., Schmitt, A., Sobel, E., and Strecker, M., 2006, Propagation of orographic barriers along an active range front: Insights from sandstone petrography and detrital apatite fission track thermochronology in the intramontane Angastaco basin, NW Argentina: Basin Research, v. 18, p. 1–26.

Cristallini, E.O., Cominguez, A., Ramos, V.A., and Mercerat, E.D., 2004, Basement double-wedge thrusting in the northern Sierras Pampeanas of Argentina (27°S)—Constraints from deep seismic reflection, *in* McClay, K.R., ed., Thrust Tectonics and Hydrocarbon Systems: American Association of Petroleum Geologists (AAPG) Memoir 82, p. 65–90.

Dahlen, F.A., Suppe, J., and Davis, D., 1984, Mechanics of fold and thrust belts and accretionary wedges: cohesive Coulomb theory: Journal of Geophysical Research, v. 89, p. 10,087–10,101.

Davila, F.M., and Astini, R.A., 2003, Early middle Miocene broken foreland development in the southern central Andes: Evidence for extension prior to regional shortening: Basin Research, v. 15, p. 379–384, doi: 10.1046/j.1365-2117.2003.00206.x.

Davis, D., Suppe, J., and Dahlen, F.A., 1983, Mechanics of fold and thrust belts and accretionary wedges: Journal of Geophysical Research, v. 88, p. 1153–1172.

DeCelles, P.G., and Giles, K., 1996, Foreland basin systems: Basin Research, v. 8, p. 105–123, doi: 10.1046/j.1365-2117.1996.01491.x.

DeCelles, P.G., and Horton, B.K., 2003, Early to middle Tertiary foreland basin development and the history of Andean crustal shortening in Bolivia: Geological Society of America Bulletin, v. 115, no. 1, p. 58–77, doi: 10.1130/0016-7606(2003)115<0058:ETMTFB>2.0.CO;2.

Deeken, A., Sobel, E.R., Haschke, M., Strecker, M., and Riller, U., 2004, Age of initiation and growth pattern of the Puna Plateau, NW-Argentina, constrained by AFT thermochronology: Amsterdam, 10th International Conference on Fission-Track Dating and Thermochronology, Abstract.

Deeken, A., Sobel, E.R., Coutand, I., Haschke, M., Riller, U., and Strecker, M.R., 2006, Development of the southern Eastern Cordillera, NW Argentina, constrained by apatite fission track thermochronology: From Early Cretaceous extension to middle Miocene shortening: Tectonics, v. 25, TC6003, doi: 10.1029/2005TC001894.

de Urreiztieta, M., 1996, Tectonique Néogène et bassins transpressifs en bordure méridionale de l'Altiplano-Puna (27°S), nord-ouest Argentina [Ph.D. dissert.]: Rennes, France, Université de Rennes I, 311 p.

Dickinson, W.R., and Snyder, W.S., 1978, Plate tectonics of the Laramide orogeny, *in* Matthews, V., III, ed., Laramide Folding Associated with Basement Block Faulting in the Western United States: Geological Society of America Memoir 151, p. 355–366.

Donelick, R.A., Ketchman, R.A., and Carlson, W.D., 1999, Variability of apatite fission track annealing kinetics: II. Crystallographic orientation effects: The American Mineralogist, v. 84, p. 1224–1234.

Dumitru, T.A., 1993, A new computer automated microscope stage system for fission track analysis: Nuclear Tracks, v. 21, p. 575–580.

Fitzgerald, P.G., Sorkhabi, R.B., Redfield, T.F., and Stump, E., 1995, Uplift and denudation of the central Alaska Range: A case study in the use of apatite fission-track thermochronology to determine absolute uplift parameters: Journal of Geophysical Research, v. 100, p. 20,175–20,191, doi: 10.1029/95JB02150.

Flanagan, K.M., and Montagne, J., 1993, Neogene stratigraphy and tectonics of Wyoming, *in* Snoke, A.W., Steidtmann, J.R., and Roberts, S.M., eds., Geology of Wyoming: Geological Society of Wyoming Memoir 5, p. 572–607.

Flemings, P.B., and Jordan, T.E., 1989, 1989, A synthetic stratigraphic model of foreland basin development: Journal of Geophysical Research, v. 94, p. 3851–3866.

Galbraith, R.F., and Green, P.F., 1990, Estimating the component ages in a finite mixture: Nuclear Tracks and Radiation Measurements, v. 17, p. 197–206.

Gallagher, K., Brown, R., and Johnson, C., 1998, Fission track analysis and its applications to geological problems: Annual Review of Earth and Planetary Sciences, v. 26, p. 519–572, doi: 10.1146/annurev.earth.26.1.519.

Garver, J.I., Brandon, M.T., Roden, T.M.K., and Kamp, P.J.J., 1999, Exhumation history of orogenic highlands determined by detrital fission-track thermochronology, *in* Ring, U., Brandon, M.T., Lister, G.S., and Willett, S.D., eds., Exhumation Processes: Normal Faulting, Ductile Flow and Erosion: London, Geological Society, p. 283–304.

Garzione, C.N., Molnar, P., Libarkin, J.C., and MacFadden, B.J., 2006, Rapid late Miocene rise of the Bolivian Altiplano: Evidence for removal of mantle lithosphere: Earth and Planetary Science Letters, v. 241, p. 543–556, doi: 10.1016/j.epsl.2005.11.026.

Grier, M.E., Salfity, J.A., and Allmendinger, R.W., 1991, Andean reactivation of the Cretaceous Salta Rift, north-western Argentina: Journal of South American Earth Sciences, v. 4, p. 351–372, doi: 10.1016/0895-9811(91)90007-8.

Gries, R., 1983, North-south compression of Rocky Mountain foreland structures, *in* Lowell, J.D., ed., Rocky Mountain Foreland Basins and Uplifts: Denver, Rocky Mountain Association of Geologists, p. 9–32.

Hilley, G.E., and Strecker, M.R., 2005, Processes of oscillatory basin filling and excavation in a tectonically active orogen: Quebrada del Toro, NW Argentina: Geological Society of America Bulletin, v. 117, p. 887–901, doi: 10.1130/B25602.1.

Hilley, G.E., Blisniuk, P.M., and Strecker, M.R., 2005, Mechanics and erosion of basement-cored uplift provinces: Journal of Geophysical Research, v. 110, B12409, doi: 10.1029/2005JB003704.

Hongn, F.D., and Seggiaro, R.E., 2001, Hoja Geológica Cachi, 2566-III, Provincias de Salta y Catamarca, República Argentina: Buenos Aires, Instituto de Geología y Recursos Minerales, Servicio Geológico Minero Argentino, v. 248, 87 p.

Horton, B.K., and DeCelles, P.G., 1997, The modern foreland basin system adjacent to the Central Andes: Geology, v. 25; no. 10; p. 895–898, doi: 10.1130/0091-7613(1997)025<0895:TMFBSA>2.3.CO;2.

Hubbard, R.J., Pape, J., and Roberts, D.G., 1985a, Depositional sequence mapping as a technique to establish tectonic and stratigraphic framework and evaluate hydrocarbon potential on a passive continental margin, *in* Berg, O.R., and Woolverton, D., eds., Seismic Stratigraphy. II: An Integrated Approach to Hydrocarbon Exploration: American Association of Petroleum Geologists Memoir 39, p. 79–91.

Hubbard, R.J., Pape, J., and Roberts, D.G., 1985b, Depositional sequence mapping to illustrate the evolution of a passive continental margin, *in* Berg, O.R., and Woolverton, D., eds., Seismic Stratigraphy. II: An Integrated Approach to Hydrocarbon Exploration: American Association of Petroleum Geologists Memoir 39, p. 93–115.

Hurford, A.J., and Green, P.F., 1983, The zeta age calibration of fission-track dating: Chemical Geology, v. 41, p. 285–317.

Isacks, B., 1988, Uplift of the central Andean plateau and bending of the Bolivian orocline: Journal of Geophysical Research, v. 93, p. 3211–3231.

Jordan, T.E., 1981, Thrust loads and foreland basin evolution, Cretaceous, western United States: American Association of Petroleum Geologists (AAPG) Bulletin, v. 65, p. 2506–2520.

Jordan, T.E., 1995, Retroarc foreland basins, *in* Busby, C., and Ingersall, R.V., eds., Tectonics of Sedimentary Basins: Cambridge, Massachusetts, Blackwell Scientific, p. 330–362.

Jordan, T.E., and Allmendinger, R., 1986, The Sierras Pampeanas of Argentina, a modern analogue of Rocky Mountain foreland deformation: American Journal of Earth Science. v. 286, p. 737–764.

Jordan, T.E., and Alonso, R.N., 1987, Cenozoic stratigraphy and basin tectonics of the Andes Mountains, 20–28 south latitude: American Association of Petroleum Geologists (AAPG) Bulletin, v. 71, p. 49–64.

Jordan, T.E., Isacks, B.L., Allmendinger, R.W., Brewer, J.A., Ramos, V.A., and Ando, C.J., 1983, Andean tectonics related to geometry of subducting Nazca plate: Geological Society of America Bulletin, v. 94, p. 341–361, doi: 10.1130/0016-7606(1983)94<341:ATRTGO>2.0.CO;2.

Jordan, T.E., Zeitler, P.K., Ramos, V.A., and Gleadow, A.J.W., 1989, Thermochronometric data on the development of the basement peneplain in the Sierras Pampeanas, Argentina: Journal of South American Earth Sciences, v. 2, p. 207–222, doi: 10.1016/0895-9811(89)90030-8.

Jordan, T.E., Schlunegger, F., and Cardozo, N., 2001, Unsteady and spatially variable evolution of the Neogene Andean Bermejo foreland basin, Argentina: Journal of South American Earth Sciences, v. 14, p. 775–798, doi: 10.1016/S0895-9811(01)00072-4.

Kay, S.M., Coira, B., and Viramonte, J., 1994, Young mafic back-arc volcanic rocks as indicators of continental lithospheric delamination beneath the Argentine Puna Plateau: Central Andes: Journal of

Geophysical Research, v. 99, p. 24,323–24,339, doi: 10.1029/94JB00896.

Ketcham, R.A., Donelick, R.A., and Carlson, W.D., 2000, A new multikinetic calibration for fission-track annealing in apatite, *in* Fission Track 2000, 9th International Conference on Fission Track Dating and Thermochronology: Lorne, Australia, p. 203–205.

Khristov, Y.V., and Mikolaychuk, A.V., 1983, Geosynclinal basement of the crust of the Fergana-Kokshaal Hercynides: Geotectonics, v. 17, no. 3, p. 233–241.

Kley, J., Muller, J., Tawackoli, S., Jacobshagen, V., and Manutsoglu, E., 1997, Pre-Andean and Andean-age deformation in the eastern Cordillera of southern Bolivia: Journal of South American Earth Sciences, v. 10, p. 1–19, doi: 10.1016/S0895-9811(97)00001-1.

Marshak, S., Karlstrom, K., and Timmons, J.M., 2000, Inversion of Proterozoic extensional faults: An explanation for the pattern of Laramide and Ancestral Rockies intracratonic deformation, United States: Geology, v. 28, p. 735–738, doi: 10.1130/0091-7613(2000)028<0735:IOPEFA>2.3.CO;2.

Mitchum, R.M., Jr., Vail, P.R., and Sangree, J.B., 1977, Seismic stratigraphy and global changes of sea level. Part 6: Stratigraphic interpretation of seismic reflection patterns in depositional sequences, *in* Payton, C.E., ed., Seismic Stratigraphy; Applications to Hydrocarbon Exploration: American Association of Petroleum Geologists Memoir 26, p. 117–134.

Mon, R., 1979, Esquéma estructural del Noroeste Argentino: Revista de la Asociacíon Geológica Argentina, v. 35, p. 53–60.

Mon, R., and Salfity, J.A., 1995, Tectonic evolution of the Andes of northern Argentina, *in* Tankard, A.J., Soruco, R.S., Welsink, H.J., eds., Petroleum Basins of South America: American Association of Petroleum Geologists Memoir 62, p. 269–283.

Penck, W., 1920, Der Südrand der Puna de Atacama. Ein Beitrag zur Kenntnis des Andinen Gebirgstypus und zur Frage der Gebirgsbildung: Abhandlungen der Säachsischen Akademie der Wissenschaften zu Leipzig, Mathematisch-Naturwissenschaftliche Klasse, v. 37, no. S, p. 420.

Phillips, S.T., 1983, Tectonic influence on sedimentation, Waltman Member, Fort Union Formation, Wind River Basin, Wyoming, *in* Lowell, J.D., ed., Rocky Mountain Foreland Basins and Uplifts: Denver, Rocky Mountain Association of Geologists, p. 149–160.

Ramos, V.A., Cristallini, E.O., and Perez, E.J., 2002, The Pampean flat-slab of the Central Andes: Journal of South American Earth Science, v. 15, p. 59–78

Ruiz, G.M.H., Seward, D., and Winkler, W., 2004, Detrital thermochronology—A new perspective on hinterland tectonics, an example from the Andean Amazon Basin, Ecuador: Basin Research, v. 16, p. 413, doi: 10.1111/j.1365-2117.2004.00239.x.

Schmidt, C.J., and Garihan, J.M., 1983, Laramide tectonic development of the Rocky Mountain foreland of southwestern Montana, *in* Lowell, J.D., ed., Rocky Mountain Foreland Basins and Uplifts: Denver, Rocky Mountain Association of Geologists, p. 271–294.

Schmidt, C.J., Astini, R.A., Costa, C.H., Gardini, C.E., and Kraemer, P.E., 1995, Cretaceous rifting, alluvial fan sedimentation, and Neogene inversion, southern Sierras Pampeanas, Argentina, *in* Tankard, A.J., Soruco, R.S., Welsink, H.J., eds., Petroleum Basins of South America: American Association of Petroleum Geologists Memoir 62, p. 341–358.

Schmitt, J.G., and Steidtmann, J.R., 1990, Interior ramp-supported uplifts: Implications for sediment provenance in foreland basins: Geological Society of America Bulletin, v. 102, p. 494–501, doi: 10.1130/0016-7606(1990)102<0494:IRSUIF>2.3.CO;2.

Sobel, E., and Strecker, M.R., 2003, Uplift, exhumation and precipitation: Tectonic and climatic control of late Cenozoic landscape evolution in the northern Sierras Pampeanas, Argentina: Basin Research, v. 15, no. 4, p. 431–451, doi: 10.1046/j.1365-2117.2003.00214.x.

Sobel, E., Hilley, G.E., and Strecker, M.R., 2003, Formation of internally-drained contractional basins by aridity-limited bedrock incision: Journal of Geophysical Research, v. 108, no. B7, 2344, doi: 10.1029/2002JB001883.

Steidtmann, J.R., McGee, L.C., and Middleton, L.T., 1983, Laramide sedimentation, folding, and faulting in the southern Wind River Range, Wyoming, *in* Lowell, J.D., ed., Rocky Mountain Foreland Basins and Uplifts: Denver, Rocky Mountain Association of Geologists, p. 161–167.

Strecker, M.R., 1987, Late Cenozoic landscape development, the Santa Maria Valley, northwest Argentina: Ithaca, Cornell University, 261 p.

Strecker, M.R., Cerveny, P., Bloom, A.L., and Malizia, D., 1989, Late Cenozoic tectonism and landscape development in the foreland of the Andes: Northern Sierras Pampeanas (26°–28°), Argentina: Tectonics, v. 8, no. 3, p. 517–534.

Strecker, M.R., Alonso, R.N., Bookhagen, B., Carrapa, B., Hilley, G.E., Sobel, E.R., and Trauth, M.H., 2007, Tectonics and climate of the Southern Central Andes: Annual Reviews of Earth and Planetary Science, v. 35, doi: 10.1146/annurev.earth.35.031306.140158.

Tapponnier, P., Lacassin, R., Leloup, P.H., Schärer, U., Zong Dalai, Wu Haiwei, Liu Xiaohan, Ji Shaocheng, Zhang Lianshang, Zhong Jiayou, 1990, The Ailao Shan/Red River metamorphic belt: Tertiary left-lateral shear between Indochina and South China: Nature, v. 343, p. 431–437.

Toselli, J.A., and Rossi, J.N., 1998, El basamento metamorfico-igneo de las Sierras Pampeanas de la provincia de Tucumán, *in* Gianfrancisco, M., Puchulu, M.E., Durango de Cabrera, J., and Aceñolaza, G., eds., Geología de Tucumán: Publicación Especial del Colegio de Graduados en Ciencias, Capitulo 5, p. 47–56.

Toselli, J.A., Lopez, J.P., and Sardi, F.G., 1999, El basemento metamorfico en Cumbres Callchaquies noroccidentales, Aconquija, Ambato y Ancasti: Sierras Pampeanas, *in* Relatorio XIV Congreso Geologico Argentino: Geologia del Noroests Argentino, p. 73–79.

Manuscript Received 4 August 2005
Revised Manuscript Received 7 September 2006
Manuscript Accepted 15 September 2006

Printed in the USA